ABSTRACT

DEVELOPMENT OF ENZYMATIC BIOFUEL CELL BASED ON CARBON NANOTUBE ELECTRODES ON POROUS SILICON

by
Fan Yang

The work presented in this thesis has focused on designing and characterizing biofuel cell electrodes using porous silicon (p-Si) as the substrate or current collecting platform on which carbon nanotubes (CNTs), both single-walled carbon nanotubes (SWNTs) and multi-walled carbon nanotubes (MWNTs), were synthesized directly, followed by enzyme catalyst immobilization on the CNTs. Laccase and glucose oxidase (GOx) were used as enzymatic biocatalysts, which were immobilized on the CNT walls and tips using an electrochemical technique. Cyclic voltammetry showed well-defined redox peaks which indicated that the enzyme (GOx and laccase) were successfully immobilized on the CNTs. The amperometric responses of the laccase electrode upon additions of bubbled air and potentiometric responses of GOx electrode to additions of glucose demonstrated that the immobilized enzymes retained their bioelectrocatalytic activity after electrochemical deposition. Working biofuel cells with p-Si/SWNTs and p-Si/MWNTs - based electrodes with immobilized enzymes were studied at room temperature in a 0.1M phosphate buffer solution of pH 7.0, containing 4 mM glucose. The peak power output of the biofuel cell with p-Si/SWNTs based electrodes was 3.32 µW at 357 mV vs. SCE (Saturated Calomel Electrode). It provided much better performance than the biofuel cell with p-Si/MWNTs electrodes, which yielded a peak power of 1.23 nW at 5.6 mV. The combination of p-Si/CNTs with redox enzymes provided a convenient prototype for a direct electron transfer, membrane-less biofuel cell.

DEVELOPMENT OF ENZYMATIC BIOFUEL CELL BASED ON CARBON NANOTUBE ELECTRODES ON POROUS SILICON

by
Fan Yang

A Thesis
Submitted to the Faculty of
New Jersey Institute of Technology
in Partial Fulfillment of the Requirements for the Degree of
Master of Science in Chemistry

Department of Chemistry and Environmental Science

January 2007

Blank Page

APPROVAL PAGE

DEVELOPMENT OF ENZYMATIC BIOFUEL CELL BASED ON CARBON NANOTUBE ELECTRODES ON POROUS SILICON

Fan Yang

Dr. Zafar Iqbal, Thesis Advisor   Date
Research Professor of Chemistry and Environmental Science

Dr. Somenath Mitra, Committee Member   Date
Professor, Acting Chair of Chemistry and Environmental Science

Dr. Carol A Venanzi, Committee Member   Date
Distinguished Professor, Graduate Advisor of Chemistry and Environmental Science

BIOGRAPHICAL SKETCH

Author: Fan Yang

Degree: Master of Science

Date: January 2007

Undergraduate and Graduate Education:

- Master of Science in Chemistry
  New Jersey Institute of Technology, Newark, NJ, 2007

- Bachelor of Engineer in Food Science,
  South China Technology of University, Guangzhou, P. R. China, 1999

Major: Chemistry

"Live as though you intend to live forever, and work as though your strength were limit less."

— S. Bernhardt

"Every person has two educations, one which he receives from others, and one, more important, which he gives himself."

— E. Gibbon

I DEDICATE THIS THESIS TO MY BELOVED FAMILY
AND
MYSELF

ACKNOWLEDGMENT

I would like to thank all those people who made this thesis possible and an enjoyable experience for me.

First of all, I would like to express my deepest sense of gratitude to my advisor Dr. Zafar Iqbal for his patient guidance, encouragement, proofreading of many thesis drafts and excellent advice during this study. I am also thankful for his generous financial support throughout my Master's study. My sincere thanks to members of my thesis committee, Dr. Somenath Mitra and Dr. Carol A Venanzi; their advice, patience, and timely support are appreciated. I am also thankful to Dr. Sergiu M Gorun, my independent study advisor; he taught me lab experimental techniques with incredible patience. I greatly appreciate Mr. Yogish Gandhi, Supervisor of the Chemistry Laboratory at NJIT, for all his kindly help. I would like to thank our group members Dr. Yubing Wang, Amit Goyal and Chi Yu, as well as all other colleagues, Dr. Cheng Li, and Yuhong Chen for their help and friendship.

Finally, I would like to express my deepest gratitude for the constant support, understanding and love that I received from my husband Ge and our parents during the past years.

TABLE OF CONTENTS

TABLE OF CONTENTS
(Continued)

Chapter | **Page**

LIST OF TABLES

LIST OF FIGURES

LIST OF FIGURES
(Continued)

CHAPTER 1

INTRODUCTION

In recent years, biofuel cells have come to prominence as more conventional fuel cell technologies have approached mass-market acceptance. Biofuel cells use the biocatalyzed oxidation of organic substances by oxygen at two electrode interfaces, which provides a means for the conversion of chemical into electrical energy. Biofuel cells are generating power from various substances, such as methanol or glucose for the oxidation processes at the anode, whereas molecular oxygen or H_2O_2 can act as the reduction substrates at the cathode. The first enzyme-based biofuel cell was reported in 1964 using glucose oxidase (GOx) [1]. Current research shows a renewed interest in biofuel cells. Instead of considering them as a general device for power generation, biofuel cells potentially offer solutions toward special power applications in implantable devices, sensors and drug delivery devices. Miniaturization is possible for biofuel cells since they use concentrated sources of chemical energy, and the fuel can even be taken from a living organism (e.g. glucose from the blood stream).

However, there are some issues that limit biofuel cells from becoming competitive in practical applications. Short lifetime and poor power density are two critical issues; they are related to enzyme stability, electron transfer rate, and enzyme loading. Thanks to the revitalization of nanoscale science and technology, many nano-structured materials, such as mesoporous media, nanoparticles, nanofibers and nanotubes have been used as efficient hosts for enzyme immobilization.

Carbon nanotubes (CNTs) can be used as biocompatible electrodes, capable of maintaining the functional properties of redox enzymes while linking biomolecules into

nanoelectronic platforms. Porous silicon was reported to be used as an enzyme carrier matrix [2]. To accomplish this deep and narrow flow channels or nanosized pores resulting in a high surface area per volume ratio were produced on porous silicon to form a micro-reactor. These micro-reactors showed a more than 100-fold increase in enzyme activity [3]. The author's objective in the work described in this thesis was to focus on the development of an enzymatic biofuel cell based on single and multiwall carbon nanotubes as electron transfer mediators fabricated on porous silicon. As far as the author is aware, this is the first time that a biofuel cell of this type has been constructed and tested.
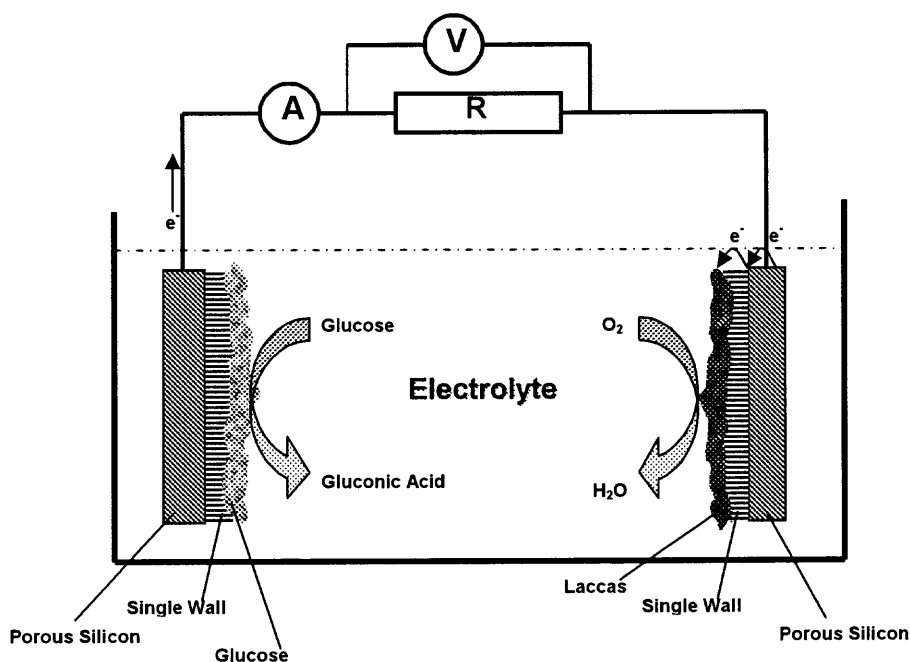
Figure 1.1 Schematic of enzyme-based biofuel cell used in author's research.

Following this introduction, details about biofuel cells will be discussed in the second chapter, including its mechanism, type, limitation and applications. The third chapter will discuss carbon nanotubes (CNTs) with their structure, synthesis method and

distinguishing properties. The fourth chapter will explain porous silicon and carbon nanotube characterization techniques such as Raman spectroscopy, and scanning electron microscopy (SEM), as well as the electrochemical electrochemistry technique of cyclic voltammetry for analyzing enzyme immobilization and their enzymatic activity. The following chapter will describe experiments involving the fabrication of porous silicon, synthesis of CNTs and enzyme deposition by an electrochemical technique. The next chapter will discuss the results and biofuel cell performance, and the conclusions and future research work in this area will be provided in the last two chapters.

CHAPTER 2

BIOFUEL CELLS

2.1 Overview

Biofuel cell research and technology development is of great interest because of its enormous potential to revolutionize small scale power sources. A biological fuel cell is a device that directly converts biochemical energy into electricity. Based on the catalytic enzymes location inside or outside of living cells, biofuel cells can be classified into microbial-based biofuel cells if living cells are involved and enzyme-based biofuel cells if no living cells are employed. Microbial fuel cells are of limited application due to their stringent working conditions, lower fuel efficiency and long-term stability owing to resistance to mass transfer across cell membranes. Enzyme-based biofuel cells use redox enzymes as biocatalysts to convert chemical energy into electrical energy and offer specific advantages over other renewable energy conversion methods.

Anode:
Glucose $\rightarrow$ Glucolactone + $2H^+$ + $2e^-$
Glucolactone + H_2O $\rightarrow$ Gluconic Acid

Cathode: O_2 + $4H+$ + $4e-$ $\rightarrow$ $2 H_2O$
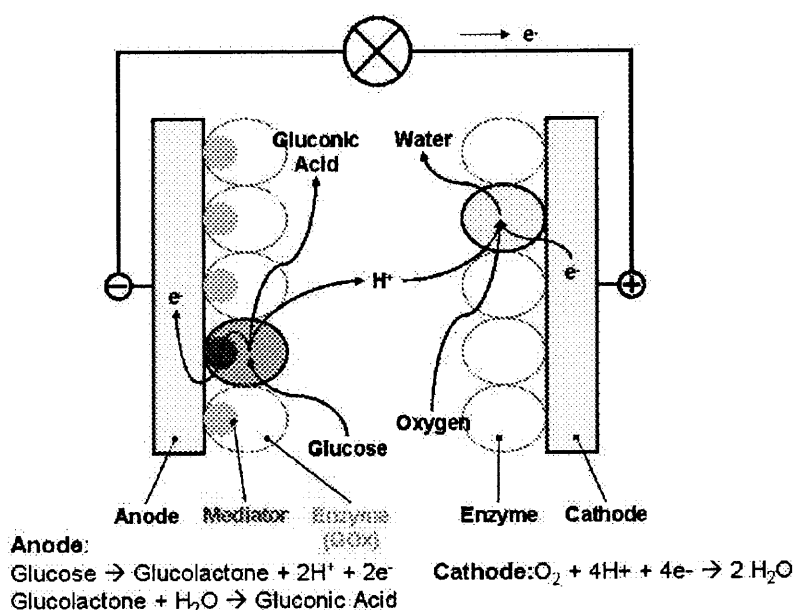
Figure 2.1 Working principles of an enzymatic glucose/oxygen biofuel cell.

The reactions in the anode chamber of the biofuel cell are the oxidation of the substrate by the enzyme and the release of electrons at the anode itself. While in the cathode chamber the hydrogen ions, which flow through an ion selective membrane and oxygen taken from the outside react to form water. Different molecular tools for electrical communication are required for different classes of oxidative enzymes. Electron transfer mediators shuttling electrons between the enzyme active centers and electrodes are usually needed for the efficient electrical communication of FAD (flavin adenine dinucleotide)-containing oxidases (e.g. glucose oxidase, GOx). From the first biofuel cell invention, several methods have been proposed and investigated in the field of bioelectrochemical technology in an effort to establish efficient electrical communication between biocatalysts and electrodes. Based on the different mechanisms, in general, electron transfer is classified into mediated electron transfer (MET) and direct electron transfer (DET) (see Figure 2.2).
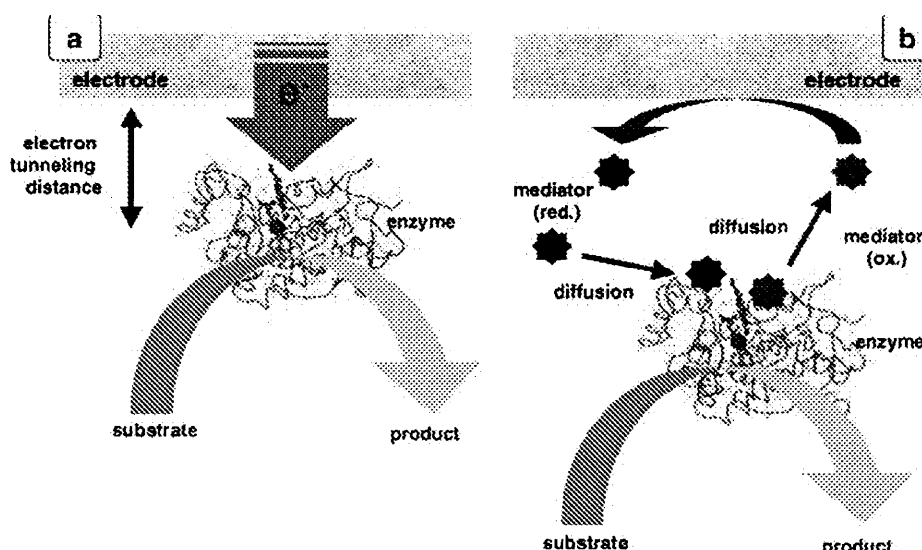
Figure 2.2 Alternative electron-transfer mechanisms. (a) Direct electron transfer (tunneling mechanism) from electrode surface to the active site of an enzyme, and (b) Electron transfer via redox mediator [4].

In MET, the electron transfer mediator works as an electron shuttle between the enzyme active site and the electrode. It acts as a co-substrate for the enzymatic reaction, and the electrochemical transformation has to be reversible. The mediator should exist a free state in solution [5], physically entrapped behind a membrane and immobilized in a matrix along with the biocatalyst [6]. In DET, the biocatalysts are directly involved in the redox reaction or reaction chain for the generation of electricity; the enzymes are immobilized on electrodes directly to facilitate the repeated use of the catalysts. One of the big challenges in developing DET biofuel cells is inefficient electron conduction between biocatalysts and electrodes.

The biofuel cell power density is usually measured by power generation per surface area of electrode, or per weight or volume of the cell [7]. The extractable power (P) of a biofuel cell is the product of the cell voltage (V) and the cell current.

$$P_{cell} = V_{cell} \times I_{cell}$$

The cell power (P) is affected by the difference in the formal potentials of the oxidizer, fuel compounds, fuel diffusivity, enzyme loading density, electrode sizes, the ion permeability, electron transfer rate etc. These different parameters collectively influence the biofuel cell power, and for improved efficiencies, the V_{cell} and I_{cell} values should be optimized.

2.2   Enzyme Based Biofuel Cell

2.2.1 Immobilization of Biocatalyst

Although enzymes are highly efficient catalysts they are difficult to incorporate into fuel cells. Early enzyme-based biofuel cells used enzyme solution instead of immobilized enzymes. However, enzymes in solution are only stable for a few days, whereas immobilized enzymes can be stable for months [8]. Enzyme immobilization can be achieved either chemically or physically. Physical enzyme immobilization is a more popular method, which has been used in most enzyme-based biofuel cell studies.

Many methods have been conducted for desirable enzyme immobilization, which contains enzymes and electron transfer molecules within an electrode volume to maintain concentration and activity. One common approach is surface adsorption, which can achieve high surface utilization by positioning mediators and biocatalysts within nanometers of the conducting surface. For example, hydrogenase and laccase enzymes have been physically adsorbed on carbon black particles to construct composite electrodes [9]. A tethered polymer brush or network is an alternative containment scheme which retains active species on a mediator surface [10]. Immobilization on polymer networks makes a bridge for dense packing of enzymes within electrode volumes at the expense of long-distance electron mediation between the enzyme's active center and a conductive surface. The efficient covalent binding of enzymes and mediators has also been studied. The strategy was to form a biocatalytic monolayer, comprising of a surface-bound mediator species that is itself bound to a single enzyme molecule [11]. For example, on the anode side, the pyrroloquinoline quinone (PQQ) mediator species has been previously immobilized on a gold surface. FAD, which is the active cofactor of the

enzyme, covalently attached to PQQ, and GOx apoenzyme (without the active center of FAD) is introduced to the PQQ-FAD layer, resulting in a physical attachment between PQQ-mediated GOx monolayer by the affinity of GOx and FAD. On the cathode side, a similar assembly is performed where cytochrome c is attached to a gold surface by site-selected covalent bonding to a maleimide monolayer [12].

2.2.2 Nanostructured Biocatalyst

Nanostructured materials have played an active role in biofuel cell development since the rapid growth of nanotechnology. Low catalytic efficiency and stability of enzymes have been seen as barriers for the development of large-scale operations to compete with traditional chemical processes. These nanostructures have large surface areas, which usually leads to high enzyme loading, resulting in improvement of power density of the biofuel cells. Moreover, enzyme stabilization in nanostructures has been reported in many papers as extending the lifetime of enzyme-based biofuel cells.

Recently, use of nanoparticles as a host for enzymes has been a growing interest. Due to the large surface area per unit mass of nanoparticles, effective enzyme loading up to 6.4 or 10 wt. % can be achieved on the nanoparticles [13]. For example, lipase was attached to γ-Fe_2O_3 nanoparticles via covalent bonds as a strategy of using magnetic nanoparticles, which avoids nanoparticle dispersion in reaction solutions because these magnetic nanoparticles can be separated from the reaction medium simply by using a magnet [14].

Nanofibers and nanotubes have more advantages compared to the more conventional inorganic nanoparticles. As mentioned above, nanoparticle dispersion in reaction solutions and subsequent recovery for reuse are difficult. The use of nanofibers

would overcome this problem while still keeping the advantage of nanometer-sized features. Electrospun nanofibers have generated much attention as supports for enzyme immobilization. Electrospinning has been proven to be an effective and economic process for the preparation of polymeric nanofibers. Bioactive nanofibers were prepared via attaching enzymes to electrospun nanofibers [15]. Carbon nanotubes (CNTs) have shown great promise in recent years for preparing enzymatic electrodes for biofuel cell applications, because it can act as a biochemically compatible, electrically conductive nanoscale interface between redox enzymes and macro-scale electrodes [16]. It has been reported that CNTs conduct electrons efficiently to promote direct electron transfer from redox enzymes to an electrode surface. The author's work has been focused on using CNTs as the electron transfer mediator via direct electrochemical attachment of the enzymes to the nanotube the sidewalls. More experimental details will be discussed in the Chapter 5.

Mesoporous materials have been extensively studied for enzyme immobilization because of their controlled porosity and high surface areas. The most frequently used approaches in immobilizing enzymes into mesoporous materials are absorbing the enzyme into the pores by controlling the pore size and charge interaction. SBA-15 (a mesoporous silicate with pore size of 5-13 nm), mesocellular foam (MCF, pore size of 15-40 nm), mesoporous carbon and mesoporous silica have been employed for rapid adsorption of enzymes. Covalently attaching an enzyme (α-chymotrypsin) to mesoporous silica showed an increase in half-life compared to that of the native enzyme.[17] In the author's work, porous silicon was used as the electrode substrate in order to take advantage of its high surface area resulting from the micro- to nano-sized pores or

channels in the material. The pores can work as local fuel reservoirs while the channels can provide the microfluidics necessary for fuel transport. The capillary action within the channels is expected to transport the fuel towards the cell's reaction sites. This can reduce the overall biofuel cell size and increase power efficiency. In addition, porous silicon is an excellent substrate for growing carbon nanotubes, which function as highly efficient electron transfer mediators and stabilizing supports for the biocatalyst.

2.2.3 Complete Enzymatic Biofuel Cell

Biofuel cells have traditionally suffered from low power densities and short lifetimes due to the fragility of the enzyme catalyst. Current efforts on biofuel cell focus on issues of catalytic rate and stability by seeking improved kinetic and thermodynamic properties in modified enzymes or synthesized enzyme-like compounds [4]. The development of materials and electrode structures is important as well in order to fully maximize the biocatalyst reaction rates in a stable environment. Finally, the whole biofuel cell system should be assessed in an operational device.

Biofuel cells are much further from commercial development than their larger fuel cell cousins, but exciting recent progress has been made [16]. For example, Heller et al created a miniature biofuel cell based on carbon fibers and operating at ambient temperature in a pH 5 aqueous solution, this miniature glucose-powered cell can produce 600 nanowatts (nW) of power. The power density of the cell exceeds by a factor of 5 the highest power density of earlier biofuel cells [18]. Later, Heller's group reported a laccase-comprising, compartment-less cell with an improved redox polymer connecting the reaction centers of glucose oxidase to the carbon fiber to produced 120 nW of power at an operating potential of 0.78V, which is the highest reported power for a miniature

membrane-less biofuel cell [19]. Researchers at Saint Louis University have developed a new biofuel cell - a battery that runs off of alcohol and enzymes - that could replace the rechargeable batteries found in everything from laptops to Palm Pilots. This ethanol/oxygen biofuel cell uses alcohol dehydrogenase to oxidize ethanol at the anode and bilirubin oxidase to reduce oxygen at the cathode; it has an active lifetime of about 30 days and shows power densities of up to 0.46 mW/cm^2 [20].

2.3   Biofuel Cell Applications

Biofuel cells can be used to produce power from waste sugars or from conventional fuels including hydrogen and alcohols. They can be used in the form of miniature cells that derive power from plants or animals to supply power to small devices.

Enzyme-based biofuel cells can be used as portable and miniature power sources for PDAs, digital cameras and similar devices. Ethanol has been used often as an alternative to the traditional fuel powered biofuel cell due to its widespread availability for consumer use, non-toxicity, and increased selectivity by alcohol dehydrogenase. For example, a microchip-based ethanol/oxygen biofuel cell was tested recently using a bioanode with a platinum cathode. This biofuel cell showed maximum open circuit potentials of 0.34 V and maximum current densities of 53.0 ± 9.1 μm^{-2}. This research demonstrates the feasibility of a microfabricated biofuel cell device [21].

The most intuitive application of enzymatic biofuel cells is for implantable power, such as microscale cells implanted in human or animal tissue or larger cells implanted in blood vessels. The benefit of an implantable biofuel cell compared to a traditional battery is one of high power density and use in a physiological environment, which can provide

infinite amounts of fuel, such as ambient sugars and oxygen. The most obvious application is to power cardiac pacemakers, which currently use a lithium-iodine battery with an operating power lifetime of about 10 years [4]. Microbial biofuel cells could be used by the military to derive power from either the fluids from trees or insects to power sensing devices.

CHAPTER 3

CARBON NANOTUBES

3.1   Overview

A single wall carbon nanotube (SWNT) can be considered to be a giant cylindrical molecule made up of only carbon atoms. The atoms on the tube walls are arranged in hexagons, the same arrangement as in graphite. An ideal carbon nanotube (CNT) can be thought of as a hexagonal network of carbon atoms that has been rolled up to make a seamless cylinder. In this way, each carbon atom is bonded to three other carbon atoms. Ideally, in the flat graphite form, carbon atoms form sp^2 bonds with neighboring atoms. This means that the 2s- and 2p-shells of each carbon atom are combined with the 2s- and 2p-shells of its neighboring atoms to form bonds that have both s and p or hybrid character.   The sp^2 bonding character can be used to approximate the bonds in the cylindrical carbon nanotubes. When the CNTs are perfect, they are of uniform diameter. This sp^2 bonding structure, which is stronger than the sp^3 bonds found in diamond, provides the individual SWNT giant molecules with their unique strength.

There are two possible high symmetry structures for SWNTs, referred to as "zig-zag" and "armchair". In practice, it is believed that a large fraction of single wall carbon nanotubes do not have these highly symmetric forms but have structures in which the hexagons are arranged helically around the tubes axis [23]. Figure 3.1 shows a small part of the irreducible wedge from an original graphene sheet from which the CNT cylinder is produced by rolling up the sheet such that the two end-points of the vector, which labeled as C, are superimposed. Each pair of integers (n, m) represents a possible tube structure (see Figure 3.2). Thus the vector C can be expressed as:

$$C = na_1 + ma_2$$

Where a_1 and a_2 are the unit cell based vectors of the graphene sheet, and $n \geq m$. It can be

seen from Figure 3.1 that m=0 for all zig-zag tubes, while n=m for all armchair tubes. All

other tubes are helical or chiral.
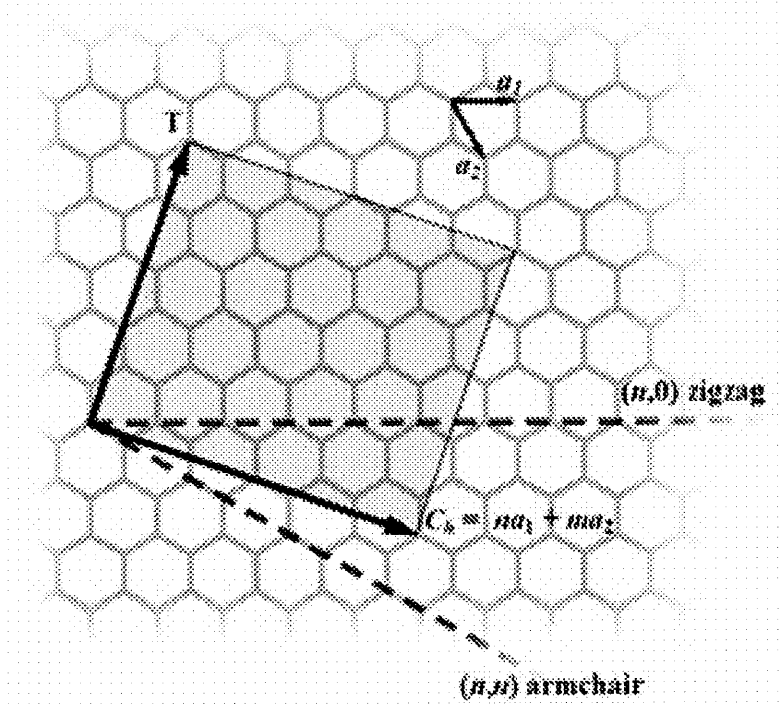
Figure 3.1 The chiral vector is defined on the hexagonal lattice as $C_h = n\hat{a}_1 + m\hat{a}_2$, where $\hat{a}_1$ and $\hat{a}_2$ are unit vectors, and n and m are integers. The chiral angle, q, is measured relative to the direction defined by $\hat{a}_1$. Zigzag nanotubes correspond to $(n, 0)$ or $(0, m)$ and have a chiral angle of $0°$, armchair nanotubes have (n, n) and a chiral angle of $30°$, while chiral nanotubes have general (n, m) values and a chiral angle of between $0°$ and $30°$ [24].

ZIGZAG
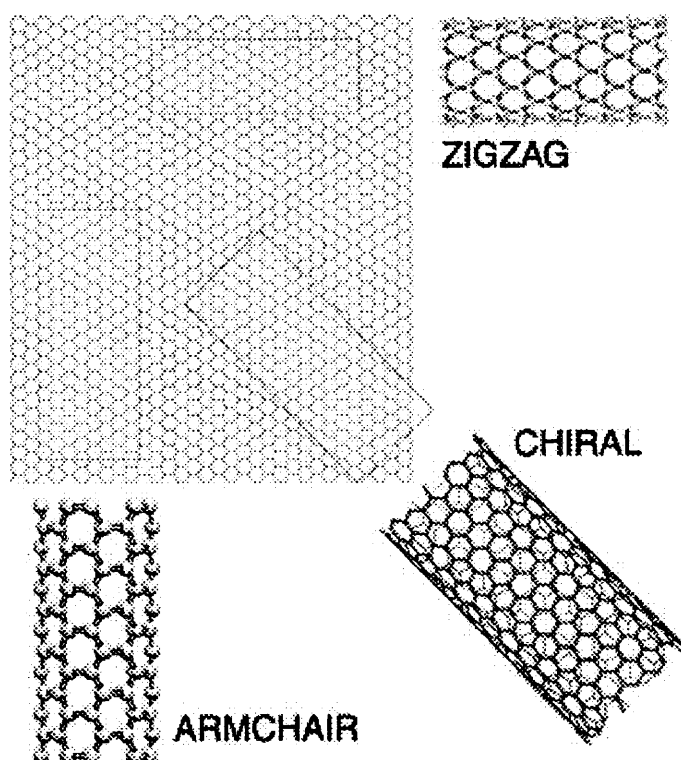
CHIRAL

ARMCHAIR

Figure 3.2 Three types of single wall carbon nanotubes referred to as armchair, zigzag and chiral nanotubes, are possible depending on how the two-dimensional graphene sheet is rolled up as shown schematically in the figure [25].

Carbon nanotubes are of two types: single-wall nanotubes (SWNTs) and multi-walled nanotube (MWNTs). SWNTs have a typical diameter of about 1-3 nm and a tube length which can be many thousands of times larger. SWNTs can be conceptualized by wrapping a one-atom-thick layer of graphite called graphene into a seamless cylinder (Figure 3.1 and 3.2). Multiwalled nanotubes (MWNTs) on the other hand have a structure consisting of multiple layers of graphene rolled into cylinders and then nested into each other as in a Russian doll to form a multiwalled cylindrical shape (see Figure 3.3). Figure 3.3 also shows the TEM image of the simplest multiwall nanotube, which consists of two walls separated by a distance of 0.34 nm corresponding closely to the inter-planar separation of graphene planes in single crystal graphite.
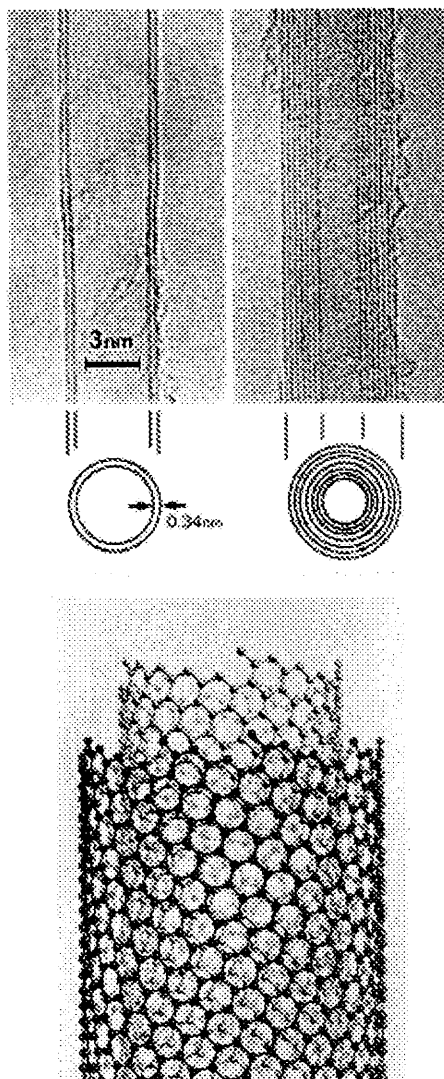
Figure 3.3 Top: TEM image of a double-wall (left) and multiwall (right) carbon nanotube. Bottom: Schematic drawing showing nesting of one tube into another to form multiwalled carbon nanotubes [26].

3.2 Synthesis of Carbon Nanotubes

Since the first report of the synthesis of multiwall carbon nanotubes in 1991 [22], much effort has been made to scale up the synthesis and elucidate the properties of these novel materials, including those of the more fundamental single wall carbon nanotubes. Electric arc discharge, laser ablation, high pressure carbon monoxide (HiPCO), and chemical

vapor deposition (CVD) techniques, have been developed to produce carbon nanotubes in sizable quantities. Large quantities of nanotubes can be synthesized by these methods, particularly by CVD and the related HiPCO techniques. Advances in catalysis and continuous growth processes are making the production of CNTs more commercially viable.

3.2.1 Arc Discharge

The first successful synthesis of CNTs was by the arc discharge technique [26]. The carbon arc discharge method, initially used for producing C_{60} fullerenes, is perhaps the easiest way to produce CNTs as it is relatively simple to undertake. The method involves an arc discharge between graphite electrodes with or without catalyst, in a vacuum chamber that is usually back-filled with inert gas (helium or argon) at low pressure (between 50 and 700 mbar), allowing a nanotube deposit to accumulate on the cathode. Nanotubes self-assemble from the resulting carbon vapor. One can form both SWNTs and MWNTs by this technique. SWNTs are formed only in the presence of catalysts [23]. However, the technique typically produces smaller than 50% volume fraction of nanotubes and requires separating nanotubes from the soot and the catalytic metals present in the crude products by extensive refluxing in strong acids.

3.2.2 Laser Ablation

Laser ablation was the first technique used to generate C_{60} and other stable fullerene clusters [27] and is now used to produce SWNTs. A graphite rod containing transition metal catalysts is vaporized by laser irradiation under an inert atmosphere and the vapors directed to a cooled quartz tube in this process; soot-containing SWNTs are produced on

the walls of the quartz tube. A gasification purification or acid reflux process is needed to remove the carbonaceous soot. Laser ablation is one of the best methods to produce high quality (typically with 70 % purity) SWNTs. Many optimization methods have been studied for high quality and purity of the SWNTs produced by the laser method. The methods include optimization of gas pressure and its flow rate, laser oven temperature, and laser parameters, such as energy fluence, peak power, continuous wave versus pulsed operation, repetition rate and oscillation wavelength [28]. However, similar to the arc-process, cost-effective scale-up of this method is difficult.

3.2.3   Chemical Vapor Deposition

Chemical Vapor Deposition (CVD) is the most attractive and commercially viable method used to grow CNTs. The growth process involves heating a catalyst material to high temperatures (500–1000 °C) in a tube furnace, then introducing a hydrocarbon gas into the tube reactor over a period of time [30]. Usually, transition metal particles are used as catalyst on a supporting matrix for growing CNTs. Nickel, iron, cobalt, molybdenum are typically used as catalysts for carbon nanotube growth. The hydrocarbon molecules are introduced into the reactor as the carbon source and catalyzed by transition metal particles to precipitate carbon around the catalyst particles to grow a tube like solid carbon structure with sp^2 bonding. This tubular carbon solid has lower energy since a tube contains no dangling bonds compared to a sheet of graphite or graphene with open edges.

Because of their relative simplicity CVD methods have great potential for scaled-up synthesis of CNTs. A number of hydrocarbons have been explored as carbon feedstock. For example, ethylene or acetylene is used for growing MWNTs at relatively

low temperatures, whereas alcohol is a good carbon source for the synthesis of high purity SWNTs at low temperatures because OH radicals produced during the synthesis etch away the amorphous carbon produced [29]. Carbon monoxide (CO) either at high pressure (also known as the high pressure CO or HiPCO process) or at atmospheric pressure is used as the carbon feedstock to grow high quality SWNTs in the 800–1200 °C temperature range [30].

3.3 Distinguishing Properties of Carbon Nanotubes

The basic structure of a CNT is built around the sp^2 hybridized C-C covalent bond with perfect alignment of the lattice along the tube axis. The closed quasi-one dimensional topology endows the tubes with unique mechanical properties, chemical specificity, ballistic electronic transport and highly efficient field emission properties.

The small diameter has an important effect on the mechanical properties of CNTs. Perhaps the most striking effect is the opportunity to associate high flexibility and high strength with high stiffness. Young's modulus and the rate of change of stress with applied strain can be used to measure the stiffness of a material [31]. The Young's modulus of the best nanotubes can be as high as 1000 GPa (1 TPa) which is approximately five times higher than steel. The tensile strength or breaking strain of nanotubes can be up to 63 GPa, around fifty times higher than steel [47].

The remarkable electrical properties of CNTs are due to the quantum confinement of electrons within the nanotubes. Electrons therefore propagate ballistically (see definition below) along the nanotube's axis and so their wavevectors point in this direction. The monolayer thickness of the graphene sheet where electrons are confined

also plays a critical role in determining the electronic properties of the CNTs. The π and

π^* states join at six points (Fermi points). In most directions of the wavevector k, such as

in the T-M direction of the Brillouin zone, the electrons encounter a semiconductor-like

band gap (see Figure 3.4). All armchair SWNTs are expected to be metallic, while one-

third of zig-zag and chiral tubes should be metallic, with the remainder being

semiconducting. In summary, a (n,m) carbon nanotube will be metallic when $|$n-m$|$=3q,

where q is an integer.

(a)   (b)
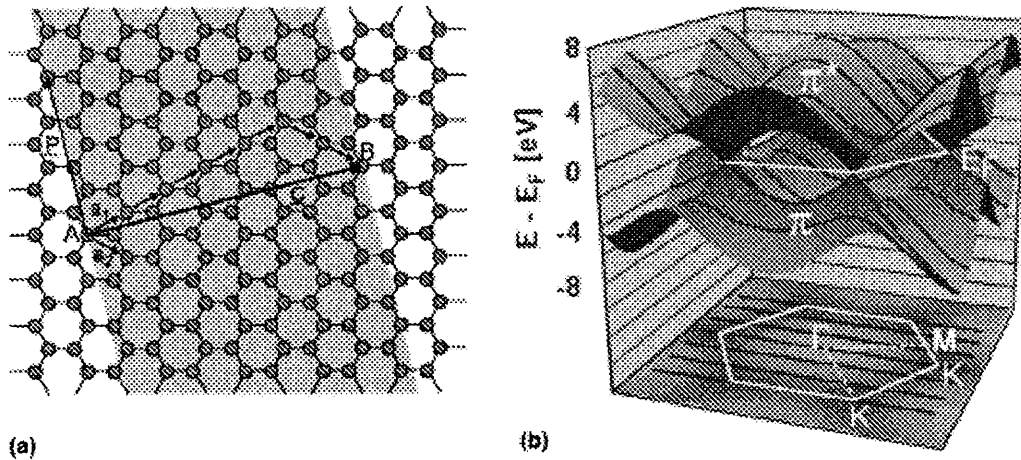
Figure 3.4 (a) Schematic drawing of the generation of a nanotube by folding of a section of a graphene sheet (left). The folding and the resulting nanotube can be characterized by a chirality vector C = na_1 + ma_2 ≡ (n, m), where a_1 and a_2 are the unit vectors of the hexagonal lattice. When point B is brought over point A a tube with a circumference C is generated. In the example shown C = 5 a_1 + 2 a_2, and the tube is labeled as a (5,2) tube. (b) Band-structure of the 2D graphene sheet (right top). The valence and conduction bands meet at six points in the Brillouin zone (K-points) lying at the Fermi energy. (Right bottom): The first Brillouin zone of a graphene sheet. The black lines represent the states of a (3, 3) nanotube. They are cuts of the graphene structure that are selected by imposing the condition that the perpendicular wavevector k_C satisfies the condition: $k_C \cdot C = 2 \pi j$, where j is an integer. If the states pass through a K-point (as in this case) the tube is a metal (that is, has no energy gap in the electronic density of states), while if they do not, the tube is a semiconductor with a small energy gap in the electronic density of states [32].

CNTs exhibit unique quantum wire properties that derive from the tubes' nanometer sized diameters in combination with the special electronic structure of a graphene sheet derived from graphite [33]. The conduction occurs through well-separated, discrete electronic states, and the quantum wire behavior is that transport along the tubes is ballistic in nature or in other words occurs with very little electron-electron scattering. Similarly all nanotubes are expected to be very good thermal conductors of phonons or vibrational excitations along the tube axis. Nanotubes therefore have low constant electrical resistivity and high thermal conductivity, and a tolerance for very high current density.

Moreover, CNTs are very stable at high temperatures in an inert atmosphere. They are also very stable in harsh chemical environments, such as in the presence of strong acids.

3.4   Communication of Carbon Nanotube Systems with Enzymes

The efficient direct transfer of electrons between enzymes and electrodes is important not only to understand the intrinsic redox behavior of enzymes, but also in developing enzyme-based biosensors and bioelectronic devices, such as enzymatic fuel cells or biofuel cells. One strategy to achieve direct electron transfer to the enzyme is to build the electrode inside the enzyme in order to contact the redox active center of the enzyme. Direct electron transfer between enzymes and electrodes is crucial to the development of mediatorless enzyme based biosensors and biofuel cells which can be used in the recycling of the enzyme back to its active form without a co-substrate. CNTs, which is as small as few nanometers in diameter with a high electrocatalytic effect and a fast

electron-transfer rate, have the potential to be such electrodes. Towards this goal, self-assembly of vertically aligned or nonaligned CNTs on an electrode surface were used to deposit enzymes on the tips or walls of the tubes.

Several oxido-reductase enzymes, such as glucose oxidase (GOx), cytochrome c, laccase, and hydrogenase, have been employed in the field of enzyme-based nanotube sensors and biofuel cells by using CNTs as molecular wires to facilitate the electron transfer of enzyme with electrode. Electrodes can be made using either MWNTs or SWNTs. Dmitri et al. reported that Toray carbon paper (TP) could be used as a platform for the growth of MWNTs followed by combination of poly-cation polyethylenimine (PEI) with negatively charged GOx, and then casting the TP/MWNT/PEI/GOx layer with Nafion solution to form a bioelectrode. Cyclic voltammograms responding to GOx modified electrodes showed redox peaks associated with direct electron transfer (DET) between the prosthetic (FAD/FADH$_2$) group bound to the apoenzyme in GOx and the MWNTs [34]. Another method involves the mixing of CNT powder or suspension with enzyme solution to create an adsorption or covalent bond attachment between the CNT sidewalls and the biomolecule [35,37,39,40]. For example, CNT suspensions lead to promotion effects on the DET of GOx immobilized on the surface or sidewalls of the CNTs. CNTs suspensions were typically obtained by dispersing the nanotubes in an aqueous solution of a surfactant, such as cetyltrimethylammonium bromide (CTAB, a cationic surfactant) [35]. SWNTs exist in metallic and semi-conducting forms with electron transport properties determined by their structures and chemical environments as discussed earlier. Nanotubes with closed tips can be opened in oxidizing environments, such as nitric acid. Open-ended nanotubes have been shown to have excellent electron

transfer properties compared to nanotubes with closed tips [36]. Typically, CNTs are treated with concentrated H_2SO_4 and/or HNO_3 to create functional groups (e.g., carboxylic acid) at the nanotube tips or sidewalls, which then react with the enzyme to form amide linkages between the amine residues of the enzymes and the carboxylic acid groups [41,42].

CHAPTER 4

CHARACTERIZATION TECHNIQUES

4.1 Raman Spectroscopy

Raman scattering is a powerful technique used to diagnose the internal structure of molecules and crystals. It is a method of chemical analysis that enables real-time reaction monitoring and characterization of compounds in a non-contact manner. It provides vibrational frequency information which is very specific for the chemical bonds in molecules. Therefore the molecules can be uniquely identified. It has found wide application in the chemical, polymer, semiconductor, and pharmaceutical industries because of its high information content and ability to avoid sample contamination.

In a Raman experiment, the sample is illuminated with a laser beam and the scattered light is collected and analyzed. The wavelengths and intensities of the scattered light are associated with molecular vibrations and can therefore be used to identify functional groups in a molecule. Raman scattered light is frequency-shifted with respect to the excitation frequency, but the magnitude of the shift is independent of the excitation frequency. This "Raman shift" is therefore an intrinsic property of the sample and provides a unique fingerprint of a molecule or crystal.

Additional information, related to the spatial form of the excitation, derives from the polarization dependence of the Raman scattered light. The shape of an excitation in a material, for example a vibration pattern of the atoms in a molecule, and the polarization dependence of the scattering, are determined by the equilibrium structure of the material through the rules of group theory. By this route one gleans valuable and unambiguous structural information from the Raman line and its polarization dependence.

Raman spectroscopy has been used in this work to characterize porous silicon. A relationship between the crystallite size and Raman frequency shift for nanocrystalline silicon, which can be extended to silicon nanocrystals within porous silicon has been established in prior work [43]. For example, single crystal Si (c-Si) displays a narrow optical-phonon band at 520 cm^{-1}. Decreasing the crystallite size to below 10 nm broadens the Raman phonon band and its frequency shifts down (Figure 4.1) due to localization of the phonons within the Si nanocrystals embedded in porous silicon [44].
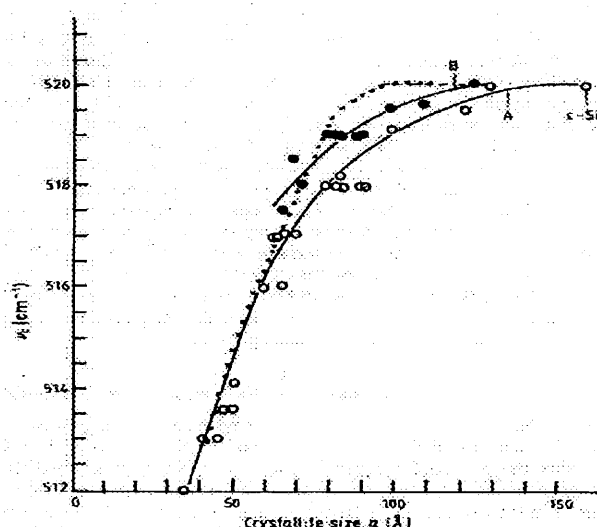
Figure 4.1 Optical Raman-active phonon frequency (v_c) for silicon as a function of crystallite size. Plot A with open circles shows the data for as-prepared nanocrystalline silicon and plot B with filled circles shows the data for annealed samples of nanocrystalline silicon. The dotted curve with crosses represents the dispersion in frequency of the 520 cm^{-1} phonon in single crystal silicon with decreasing crystallite size or increasing wave vector within the Brillouin zone. [45].

Raman spectroscopy is also a useful and powerful technique to characterize SWNTs. Raman scattering in carbon nanotubes involves strong resonances of the incoming and outgoing light and the vibration states with the one-dimensional electronic

energy states of a tube. This technique can probe several characteristics of carbon nanotubes.

The RBM (radial breathing mode) frequencies ω_{RBM} appearing between 120 cm^{-1} and 250 cm^{-1} for SWNTs with tube diameters (d_t) between 1 nm and 2 nm correspond to the vibration of the C atoms in the radial direction, as if the tube was breathing.

RBM frequencies are generally given by the empirical relationship: $\omega_{RBM} = A/d_t + B$, where d_t is the average diameter of an individual nanotube and A and B are empirical constants [46]. When the SWNTs are bundled: $A = 234$ cm^{-1} nm and $B = 10$ cm^{-1}. For isolated SWNTs: $A = 248$ cm^{-1} nm and $B = 0$. The tangential modes referred to as the G (graphitic) band (between 1500-1600 cm^{-1}) correspond approximately to the C-C stretching mode. They provide a signature of SWNTs and also distinguish between metallic and semiconducting SWNTs. The SWNTs show a characteristic double-peak structure in the G mode region, and when metallic tubes are predominant there is a broadening of the lower frequency G line due extensive coupling of the C-C stretching vibrational modes with the conducting electrons. The so-called D (disorder) band (around 1350 cm^{-1} with 488 nm laser excitation) gives a measure of the density of defects on the tube walls or presence of disordered carbon in the sample.
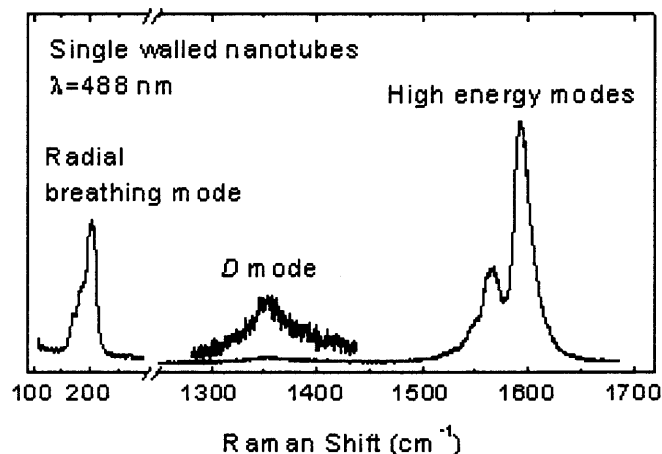
Figure 4.2 Raman spectrum of a semiconducting single walled carbon nanotube.

4.2   Scanning Electron Microscopy

Scanning electron microscopy (SEM) is one of the most powerful techniques for producing high resolution images of a sample surface. The images with high resolution at high magnification (up to 300kX) provide the material's surface morphology information which can be visually interpreted. For typical instruments, structures down to the order of 2 to 5 nm can be observed.

In this thesis, the surface structures of the porous silicon samples fabricated were examined by the SEM technique, which provided high resolution images of the sample porosity. In the case of carbon nanotubes, SEM images can be used to check the bulk yields of bundled SWNTs. High resolution images (above 50,000x magnification) can be used to identify SWNTs and MWNTs based on their structural morphology. Individual SWNT and SWNT bundles are typically either very straight or uniformly curved, whereas CVD grown MWNTs have large diameter, disorder on the sidewalls and coiled structures with bamboo-like nodes. Alignment of carbon nanotubes perpendicular to the substrate can also studied by the SEM technique by imaging in the sample tilting mode.

4.3   Cyclic Voltammetry

Cyclic voltammetry (CV) is an electrolytic method that uses microelectrodes and an unstirred solution so that the measured current is limited by analyte diffusion at the electrode surface. In a cyclic voltammetry experiment, as in other controlled potential experiments, a potential is applied to the system, and the Faradaic current response is measured (a Faradaic current is the current due to a redox reaction). The electrode potential is ramped linearly to a more negative potential, and then ramped in reverse back to the starting voltage. At a critical potential during the forward scan, the electroactive species will begin to be reduced, after reversal of the potential scan direction and depletion of the oxidized species, the reverse oxidation reaction, takes place. This provides a fast and simple method for characterization of a redox-active system and an estimate of the redox potential. In addition it can also provide information about the rate of electron transfer between the electrode surface and the analyte. In this biofuel cell work, the author used CV extensively to study the electroactivity of the fabricated biocatalysts.

CHAPTER 5

EXPERIMENTAL WORK

5.1   Materials and Apparatus

5.1.1 Materials

The following materials were used: (1) Silicon wafer, n-doped (1,1,1), resistivity, ~ 0.005 ohms-cm, thickness of 625 +/- 25 μm; from Silicon Inc. ID, US; (2) Hydrofluoric acid (HF), 48~51%, from Acros; (3) Cobalt(II) nitrate, 99.3%, from Sigma; (4) Ammonium heptamolybdate tetrahydrate, 99.98%, from Aldrich; (5) Glucose oxidase (Type VII, from Aspergillus niger, 200U(?)/mg), from Sigma; (6) Laccase (from Agaricus, 7.59U/mg), from Sigma; (7) β-D(+) Glucose (97%, remainder primarily α – anomer), from Sigma; and (8) Buffer solution (0.05M, potassium phosphate monobasic-sodium hydroxide, pH 7.00), from Fisher Chemicals. All chemicals were of analytical grade.

5.1.2 Equipment Used

Porous silicon (p-Si) preparation was performed by an electrochemical technique using a HP 6234 dual output power supply. Raman spectroscopy and scanning electron microscopy (SEM) were typically used for the characterization of the CNTs and p-Si samples prepared. Micro-Raman spectroscopy were carried out using a Horiba/Jobin Yvon LabRaman system with a scanning stage attachment, cooled CCD (charge coupled device) detection and 632.8 mm He-Ne laser excitation. Micro-Raman data recorded were always at various regions of the sample. SEM imaging was carried out using a LEO 1530 field emission instrument. All cyclic voltammetry (CV) curves were recorded by a potentiostat cell using an ELECHEMA, MODEL PS-205B potentiostat – galvanostat

with a three electrode system consisting of the working electrode, a platinum wire auxiliary electrode and a saturated calomel electrode (SCE) as the reference electrode.

5.2   Porous Silicon Fabrication

Ever since Canham [48] reported on the light emission of porous silicon (p-Si) at room temperature, considerable attention has been given to the emission mechanism; however, the mechanism remains unclear. Canham explained it on the basis of the effect of the quantum confinement of electrons in nano-sized silicon particles resulting in the creation of a direct band gap, where efficient direct light emission is permitted without phonon assistance. Alternate chemical mechanisms have also been proposed which are consistent with some of the experimental data.

Besides the optoelectronic properties of p-Si, other properties, such as high surface reactivity, high specific surface area or biocompatible properties, make this material highly useful for applications in biosensors and as a therapeutic material [49].

P-Si is produced by non-uniform electro-etching of silicon with an electrolyte containing hydrofluoric acid. The etching results in a system comprised of a disordered distribution of pores with nanocrystals remaining in the inter-pore regions. P-Si can be classified as microporous (with a pore size greater than 50 nm), mesoporous (pore size of 5-50 nm) or nanoporous (pore size less than 5 nm). The internal surface of p-Si per unit volume can be very large, or on the order of $500 m^2/cm^3$. In this work, the morphology of p-Si was investigated by scanning electron microscopy whereas Raman spectroscopy was used to determine the crystallite sizes of the nanocrystals in the inter-pore regions.

Pristine silicon wafers ($\sim$ 1 cm^2 in area) were used to fabricate porous silicon by an anodic etch in ethanolic HF solution, HF/ethanol 1:1 (v/v) in a set-up similar to that shown schematically in Figure 5.1. It was anodically biased and the etching was done by controlling the current density at 200mA/cm^2 for 30 minutes. The etched Si wafer was bathed in pure ethanol for half an hour to release the extra hydrogen bubbles formed within the pores. Distilled water was used to wash away excess ethanol and reduce the strong capillary tension, since water is non-miscible with the surface layers of p-Si. The fabricated p-Si sample was then dried in air at room temperature, after which it remained stable and did not exhibit cracking.

Pt (Cathode)   Si (Anode)

HF/ethanol

Teflon
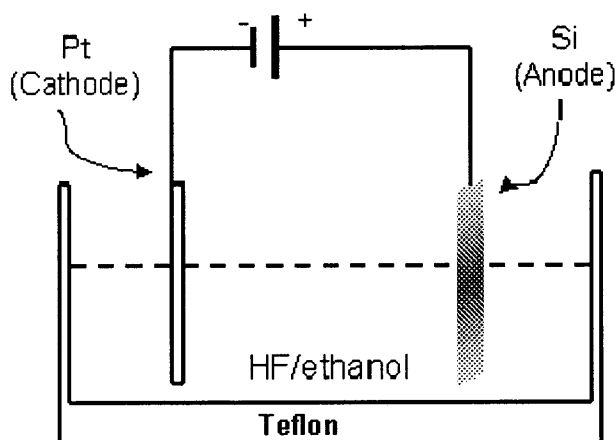
Figure 5.1 Schematic diagram of porous silicon fabrication by electrochemical etching.

In this study, p-Si was prepared for use as the platform or substrate on which the CNT electrodes were grown. P-Si also functions as the current collector and flow field for the biofuel (in this case glucose). The porosity developed in porous silicon functions as micro-capillaries, wicking structures and as built-in fuel reservoirs. The fuel can be pumped towards the cell's reaction sites by the capillary action of the micro-pores of p-

Si. The capillary driving pressure across the porous electrode increases with decreasing pore diameter [50].

5.3   Synthesis of Carbon Nanotubes on Porous Silicon

The synthesis of CNTs was modified following the method developed by Wang [51]. Cobalt (Co from cobalt (II) nitrate) and molybdenum (Mo from heptamolybdate tetrahydrate) with 1:1.5 in atomic weight ratio was used as bimetallic catalyst / promoter for the growth of CNTs. The catalysts / promoter precursor solution was prepared using 0.05 wt% and 0.075 wt% of Co and Mo metal to 1 wt% of polyvinyl pyrollidone (PVP) in 90% ethanol. PVP helps to immobilize the catalyst / promoter particles. In preparing the catalyst / promoter precursor solution, cobalt nitrate and ammonium heptamolybdate tetrahydrate were first dissolved in water. PVP was then added and dissolved in clear cobalt and molybdate salt solution, and then nine times by volume of pure ethanol in water was added to the solution. The catalyst / promoter precursor was deposited on porous silicon by spin coating at 2000 rpm for 40 seconds. Following this PVP was removed by annealing at 700°C in air at a heating rate of 1°C/min, and holding at 700°C for 1.5 hours. The catalyst coated p-Si substrate was placed in a quartz boat, which was then positioned in a quartz tube inside an electric furnace as shown schematically in Figure 5.2.

The temperature was held at 700°C for 40 minutes to form the bimetallic catalyst / promoter by reduction under H_2 flowing at 100 sccm (standard cubic centimeters per minute). The reaction tube was evacuated before the carbon source, pure alcohol, was introduced using Ar flowing at 300 sccm for 10 minutes as the carrier gas. After cooling

down under pure Ar flow, the porous silicon substrate with the grown carbon nanotubes was taken out for analysis by scanning electron microscopy (SEM) and Raman spectroscopy.
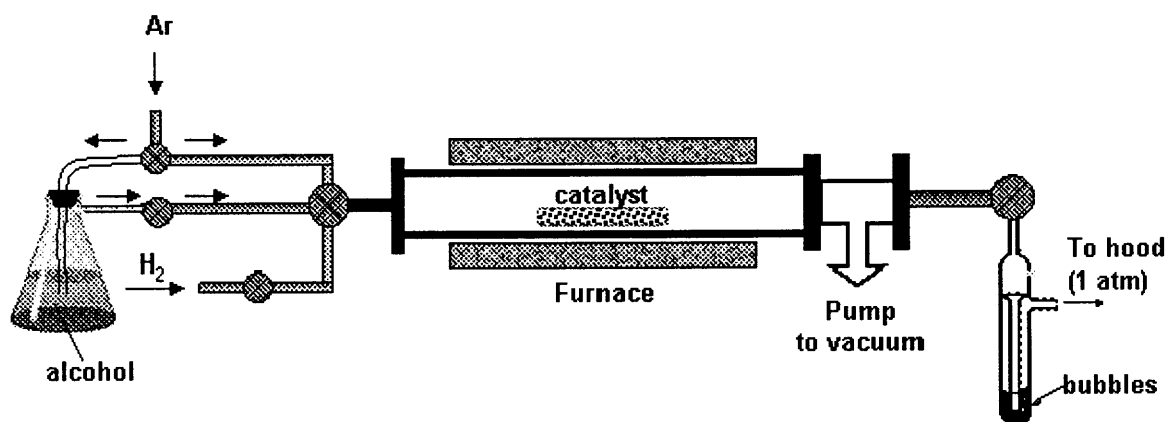
Figure 5.2 Experimental set up for the growth of CNTs on porous silicon used in this work.

5.4 Enzyme Deposition and Immobilization on Carbon Nanotubes

The carbon nanotubes on the p-Si substrates were functionalized with carboxyl groups by sonication in concentrated HNO_3 for 5 minutes followed by washing with distilled water for 10 minutes at room temperature. This procedure is well known to functionalize the tube tips and sidewalls with carboxylic groups. After washing the substrates were dried in air. The method used was a modified version of the procedure reported by Liu et al [52].

Figure 5.3 Immobilization of GOx based on p-Si/CNT substrate.

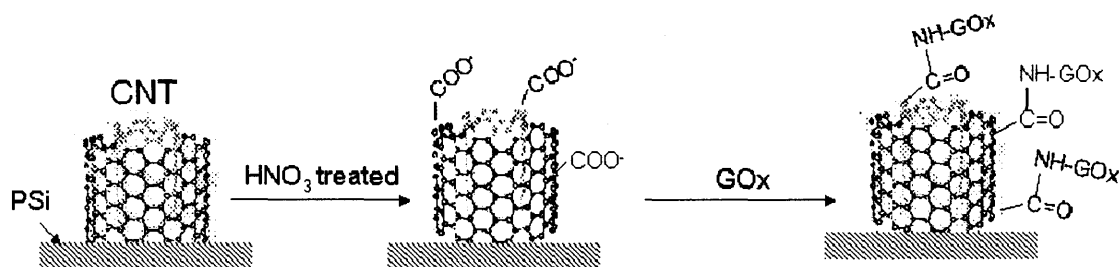Electrochemical reactions were performed with an ELCHEMA PS 205B Potentiostat / Galvanostat system using a conventional three electrode cell, which included the p-Si/CNTs working electrode, platinum counter electrode and SCE reference electrode. Cyclic voltammetry (CV) was used to demonstrate reduction-oxidation reactions as well as electrical energy generation (see Figure 5.3). The working electrolyte solution was 20 ml pH 7 buffer containing 20 mg of enzyme, GOx for anode or laccase for cathode. The swept potential was from -1 V to 1 V and then back to -1 V. All electrochemical experiments were carried out at an ambient temperature of 25°C.

Current or potential response to enzymatic redox reaction was demonstrated by chronoamperometry and chronopotentiametric methods, which were also carried out by the ELCHEMA PS 205B Potentiostat / Galvanostat. A conventional three electrode setup was used. In order to analyze the catalytic activity of the immobilized GOx, the p-Si/MWNTs/GOx electrode was used as the working electrode; platinum wire and SCE reference electrodes were used as the counter electrode and reference electrode respectively. The electrolyte comprised of 0.1M KCl and 5 mM glucose in 20 ml pH 7.0 phosphate buffer. Potentiometric responses of the p-Si/MWNTs/GOx electrode with successive additions of 5mM glucose were recorded. The half cell set up was also used for measuring the catalytic activity of the laccase modified electrode. Electrocatalytic

reduction of O_2 at the p-Si/MWNTs/laccase electrode was studied by chronoamperometry using 0.1M KCl in pH 7.0 phosphate buffer as the electrolyte upon additions of 2ml of bubbled air.

CHAPTER 6

RESULTS AND DISCUSSION

6.1   Characteristics of the Porous Silicon Samples

The surface morphologies of porous silicon were studied by SEM and Raman spectroscopy to determine the crystalline sizes of the nanoscale silicon in the p-Si samples. The SEM image in Figure 6.1 showed that the pore sizes were about 20 nm. More detailed information regarding the crystalline sizes of the nanostructured regions were obtained by Raman spectroscopy. Different regions were analyzed by Raman spectroscopy and the Raman shifts shown in Figure 6.2 were found to be between 513 cm^{-1} to 516 cm^{-1}, which correspond to silicon nanocrystalline sizes between 5-8 nm [45].
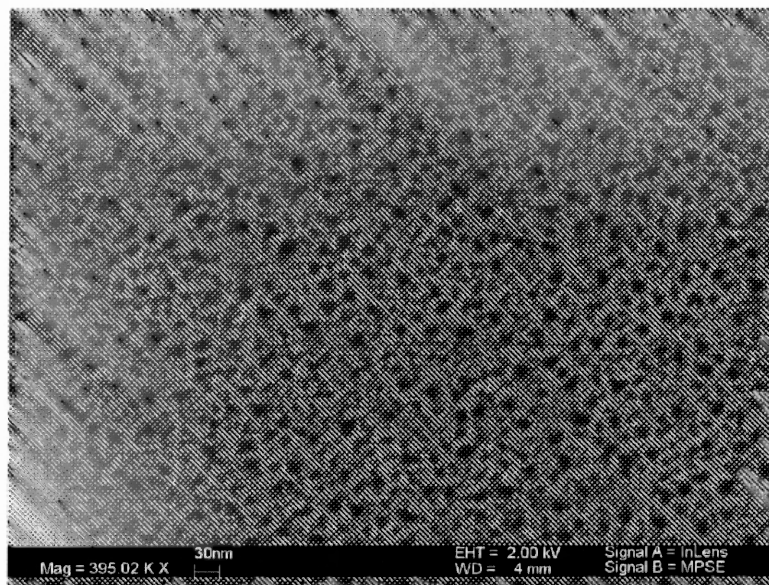

Figure 6.1   SEM image of a typical porous silicon sample fabricated in this work, the scale bar is 30nm.
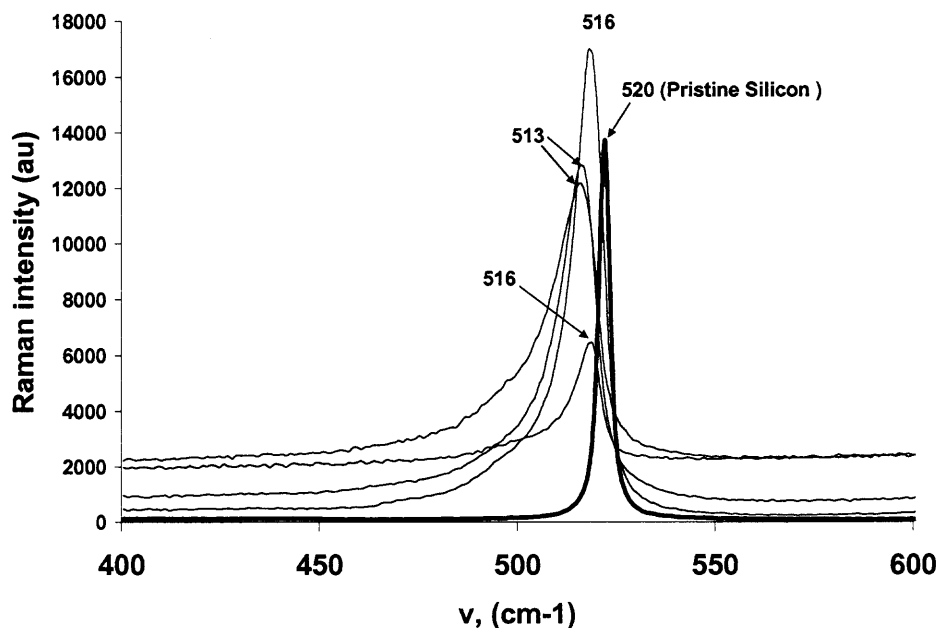
Figure 6.2 Raman spectra from different regions of a porous silicon sample.

6.2 Characteristics of Carbon Nanotubes on Porous Silicon

Catalyst can be deposited on a substrate by dry or wet methods. In the dry method, thin films of catalyst are sputtered onto the substrates [54]. Wet methods typical involve depositing catalyst precursors from an aqueous solution of the precursors. Here wet methods were used for synthesis of the CNTs on p-Si. The particle size distribution of the catalytic nanoparticles is difficult to control on porous silicon surfaces since the particles are obtained by decomposition of the deposited precursor films. Therefore it is difficult to obtain SWNTs in a controlled manner using the alcohol CVD method; as a result, either SWNTs or MWNTs was produced. However, high densities of either SWNTs or MWNTs, were easily obtained by using p-Si as substrate (see SEM images in Figure 6.3 and 6.4). Based on experimental observations it was found that the p-Si surface with nano-sized pores prevented catalyst nanoparticles from migrating and sintering at

elevated temperatures, which enhanced the yield of the CNTs [55]. From the SEM image of MWNTs (see Figure 6.3), the p-Si substrate was almost fully covered by CNTs. Visual observation indicated that the tubes had diameters in the 20-50 nm range with lengths around 1 μm. SWNTs deposited on p-Si were analyzed by SEM and Raman spectroscopy (see Figures 6.4 and 6.5). The SEM image showed that the p-Si substrate was covered by a thick layer of SWNTs; the tubes were knitted together and tended to lie over the porous silicon surface with lengths up to several microns.
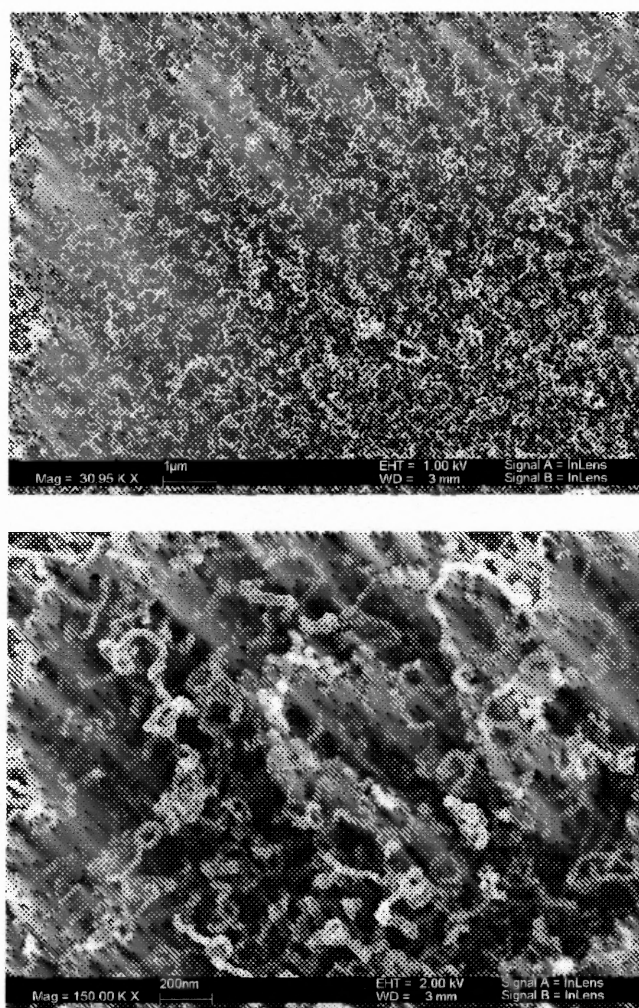

Figure 6.3 SEM images taken at low (top) and high (low) resolution of MWNTs as grown on p-Si., The scale bars are 1 μm and 200 nm, respectively.
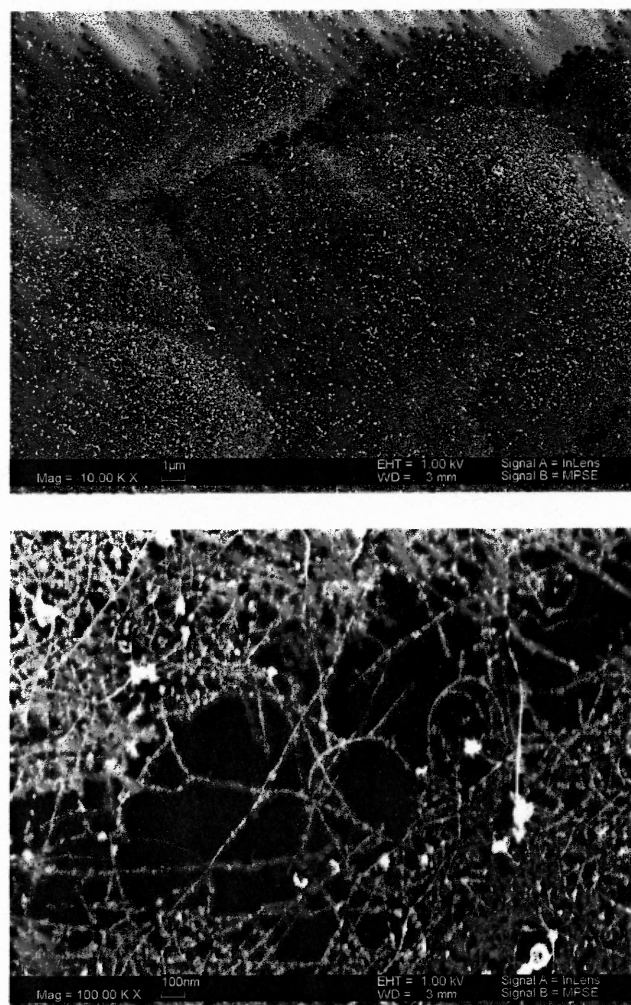
Figure 6.4 SEM images taken at low (top) and high (low) resolution of SWNTs as grown on p-Si magnification. The scale bars are 1 μm and 100 nm, respectively.
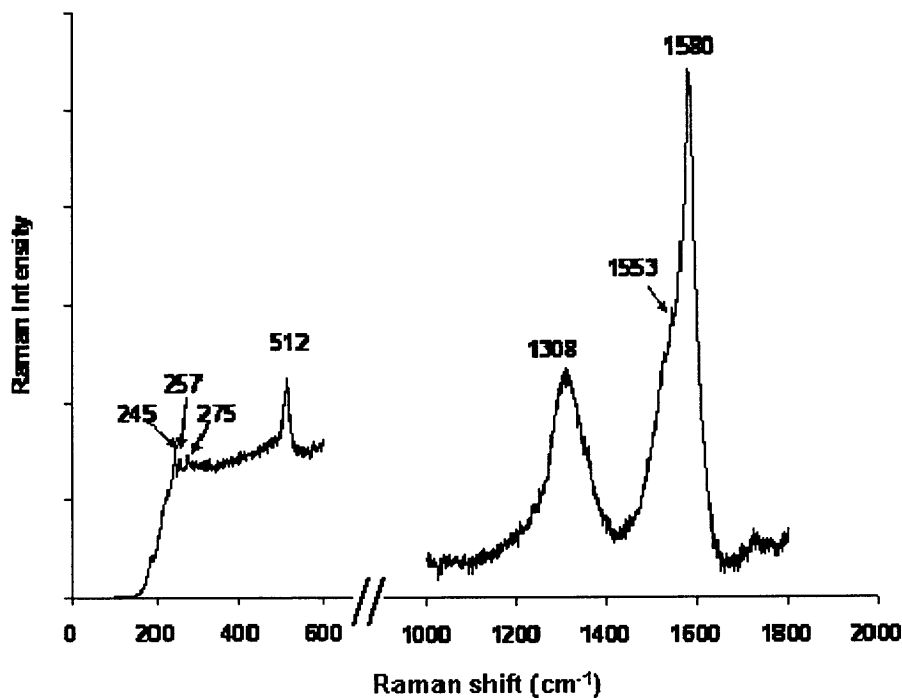
Figure 6.5 Typical Raman spectrum of SWNTs on p-Si prepared in this work.

As discussed earlier, Raman spectroscopy is a highly specific method for analyzing SWNTs. The Raman spectrum (Figure 6.5) taken from the nanotubes on p-Si showed the characteristic narrow G band at 1580 cm^{-1} of SWNTs with a second component at 1553 cm^{-1}. The D mode at ~ 1300 cm^{-1} associated with disordered carbon and/or defects and the radial breathing modes (RBM) around 150 – 300 cm^{-1} are also typical features of the Raman spectra of SWNTs. The average diameter of the individual SWNTs in a bundle was around 1 nm as estimated using the equation: v_{RBM} (cm^{-1}) = α / d (nm), where α =248 cm^{-1} [56].

6.3   Characteristics of Enzyme Immobilization

6.3.1 GOx Immobilization

Among all the enzyme-based biofuel cells, glucose modified electrodes are the most widely studied because they are inexpensive and easy to obtain from natural sources. GOx catalyzes the oxidation of glucose to gluconic acid as shown below (Figure 6.6).

Glucose + Oxygen $\xrightarrow{\text{GOx}}$ Gluconic acid + Hydrogen Peroxide
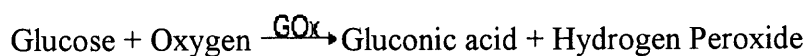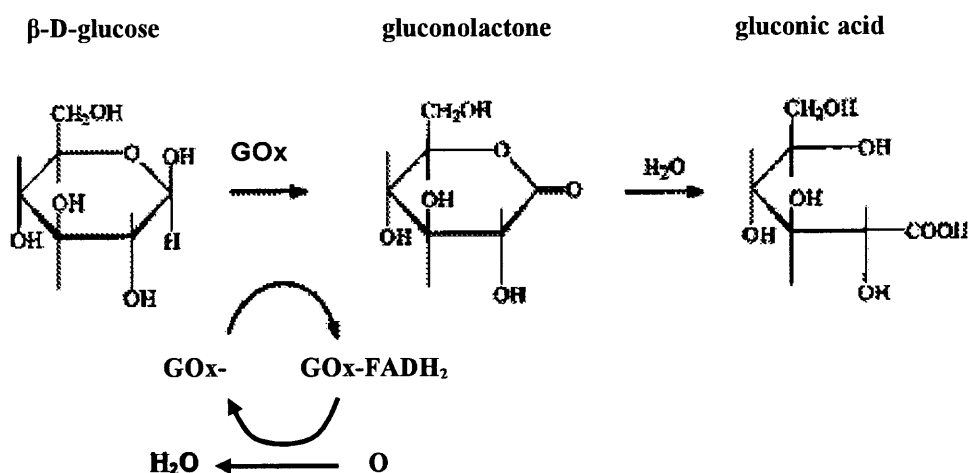
Figure 6.6   Glucose oxidase (GOx) catalyses the oxidation of glucose to gluconic acid and hydrogen peroxide, using molecular oxygen as the electron acceptor [59].

Flavin adenine dinucleotide (FAD) is the cofactor of GOx and it is a common component in biological redox reactions. FAD works as the initial electron acceptor and is reduced to FADH$_2$ with a gain of an electron from a nearby molecule (see Figure 6.7). The minimum distance between the flavin and the surface of the GOx monomer is 13 Å.
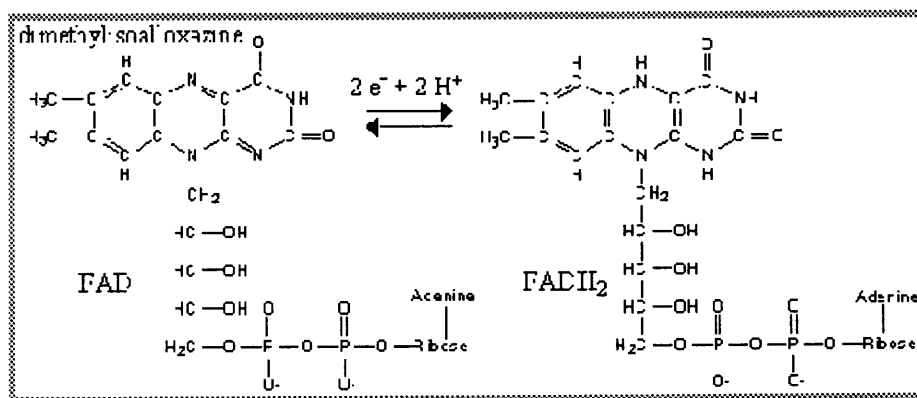
Figure 6.7 FAD is the prosthetic group that functions as an electron acceptor, the reduced FAD accepts a second H^+, yielding $FADH_2$ [60].

Electrochemistry deals with the cell potential as well as the energy of chemical reactions. In a redox reaction, the energy released due to movement of charged particles gives rise to a potential difference. The process of GOx immobilization onto CNTs involves a coupled chemical and electrochemical reaction. GOx attachment with CNTs occurs via the amide linkages between the amine residues in GOx with the carboxylic acid groups on the CNT sidewalls and tips. It can be represented as CE (Chemistry and Electrochemistry) reaction as follows:

C   CNTs-COOH + GOx(FAD) $\longrightarrow$ CNTs-CONH-GOx (FAD)

E   CNTs-CONH-GOx (FAD) + 2e$^-$ $\longleftrightarrow$ CNTs-CONH-GOx (FADH$_2$)
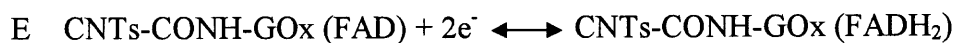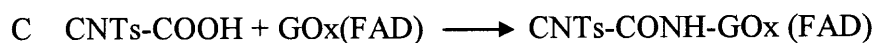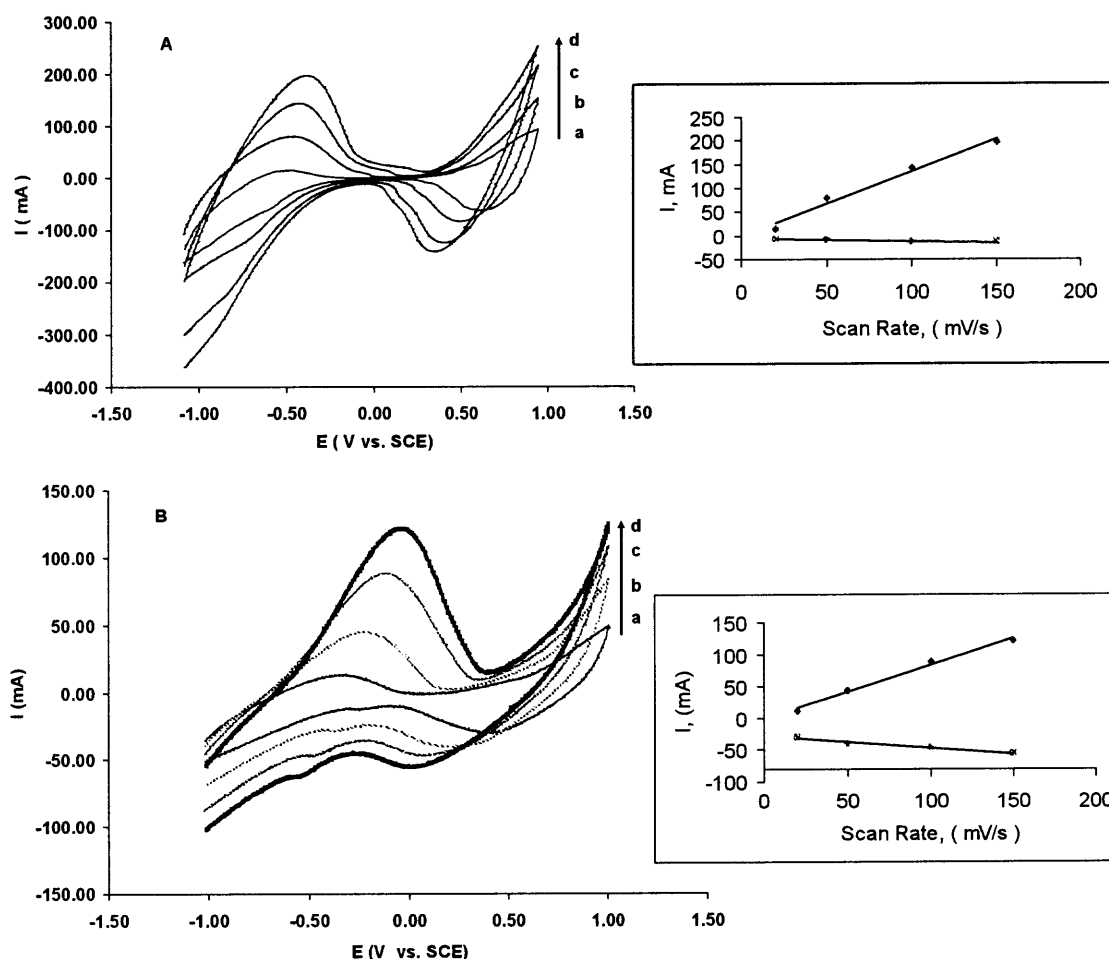
Figure 6.8 CV curves for GOx deposition and the plots of redox peak currents versus scan rate on p-Si/MWNTs substrate (A) and p-Si/SWNTs substrate (B) at various scan rates (mV/s): a. 20, b. 50, c. 100, d. 150 mV/s. p-Si/CNTs substrates were in 20 ml buffer solution at pH=7.0, with 1mg/ml GOx.

From the CVs (see Figure 6.8), the well-defined redox peaks observed indicated successful GOx attachment on both p-Si/MWNTs and p-Si/SWNTs substrates. For a redox monolayer modified electrode, the peak potentials can be represented by the separation between the peak potentials: $\Delta E_p = E_{pa} - E_{pc} = 59$ mV/n (for a reversible reaction, where n is number of electrons transferred) and the formal potential of the redox process: $E^\circ = (E_{pa} + E_{pc})/2$

The CV curves were run from higher to lower scan rates, it can be seen that the peak current increases and shifts with increasing scan rate resulting in larger separation potential ΔE_p. The observed ΔE_p values were larger than expected for a reversible one-electron reaction (ΔE_p 59 mV [57]) for p-Si/MWNTs and p-Si/SWNTs substrates, indicating that the electron transfer rate was low, i.e. that the process was quasi-reversible. The linear relationship of the peak current with the scan rate showed that the adsorbed GOx performed as a surface-confined electrode reaction. The formal potential of $FAD/FADH_2$ redox coupled at -460 mV (vs. SCE) at pH 7.0 (25 °C) [58]. While the formal potential $E°$ of p-Si/MWNTs/GOx and p-Si/SWNTs/GOx were -30 mV and -20 mV respectively vs. SCE, which were positive relative to the formal potential of the $FAD/FADH_2$ redox reaction. This is because: 1) The chemical reaction occurred during potential sweeping resulting in slower kinetics of the electrochemical reaction and thus equilibrium was not established rapidly enough (in comparison to the voltage scan rate); 2) The redox peak shift with increasing scan rate may be due to change of the GOx concentration in the electrolyte solution in the process of GOx immobilization; 3) The p-Si substrate experienced high temperature of 700 °C in air for a short time during catalyst formation for CNT growth resulting in poor interfacial conductivity due to oxide formation which reduced the electron transport efficiency; and 4) The depth of the redox center for GOx is about 13 Å, so the electron transfer rate between the active site of GOx and the electron surface is usually slower than for the redox reaction of pure $FAD/FADH_2$, as a result of the more positive formal potential range.

Multiple scan rate cyclic voltammetry of p-Si/MWNT/ GOx showed that the redox peak separation potential ΔE_p changed from 672 mV at 150 mV/s to 1000 mV at

20 mV/s. The variable scan rate CVs of the p-Si/SWNT/GOx showed ΔE_p of 20 mV at 150 mV/s, 150 mV at 100 mV/s, 468 mV at 50mV/s to 735 mV at 20 mV/s, which were smaller compared to the p-Si/MWNT/ GOx electrode. Here SWNTs were found to be favorable for fast electron transfer between the p-Si/CNT electrode and GOx compared to a similar electrode constructed out of MWNTs, since SWNTs with tiny diameters were more accessible to the cavity of the active site in GOx to build an efficient electron transfer channel. Also the larger surface area of SWNTs with functional carboxylic groups could hold more GOx molecules via amide linkages. However, the large separation potential measured under the conditions used here suggests that the globular protein shell of GOx was still an obstacle and the system will need further optimization (such as coating the p-Si interfaces with gold to increase electrical conductivity and prevent oxidation) for improved electron transfer of the enzyme to the electrode. In addition, further increase in the enzyme loading on the CNTs would be necessary.
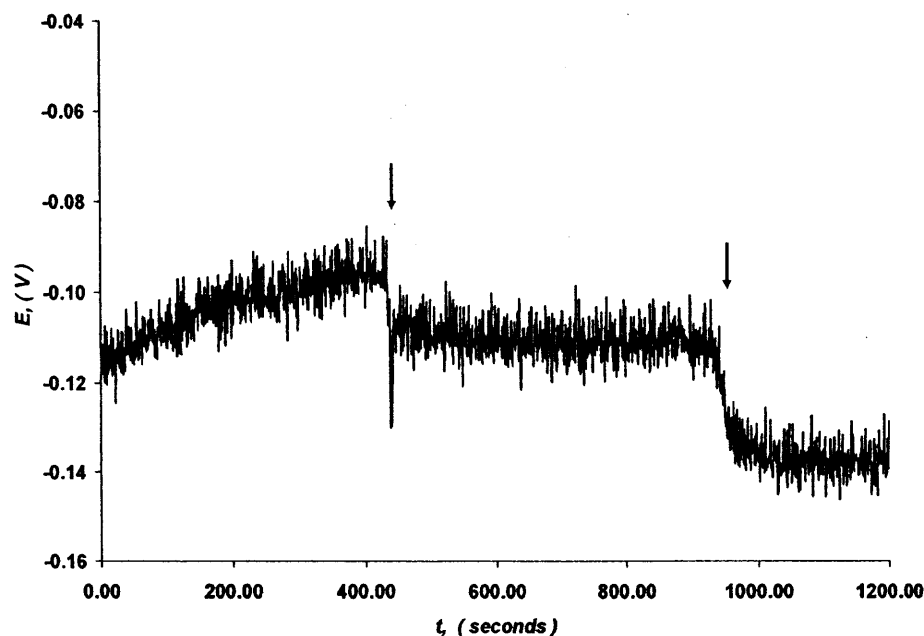
Figure 6.9 Potentiometric responses of p-Si/MWNT/GOx electrode at 600 mA in 20 ml pH 7.0 phosphate buffer, 0.1 M KCl with the initial 5 mM glucose upon additions of 5 mM glucose.

A chronopotentiometric experiment at a constant current of 600 mA was carried out for a p-Si/MWNT/GOx electrode under constant stirring (see Figure 6.9). The potential showed sharp increases with injections of millimolar concentrations of glucose (fuel) indicating that the electrode can be used as a glucose sensor. GOx was able to simultaneously undergo direct electron transfer with the electrode and to retain its catalytic activity, as shown by the bioelectrocatalytic activity of GOx immobilized on the surface of p-Si/MWNTs modified electrodes in the presence of glucose.

6.3.2 Laccase immobilization

Laccases are copper containing enzymes formed by a highly glycosylated single peptide chain (110 kDa, 45% carbohydrate content) containing one set of Cu centers. Laccases contain one type 1 (T1) Cu center, one type 2 (T2) Cu center, and one type 3 (T3) Cu

center. The T2 and T3 sites form a trinuclear Cu cluster on which O_2 is reduced. It is widely believed to be the simplest representative of the ubiquitous blue multi-copper oxidase family, which catalyze the oxidation of *ortho-* and *para*-diphenols, aminophenols, aryl diamines, polyphenols, polyamines, lignin as well as some inorganic ions coupled to the reduction of molecular dioxygen to water [61].
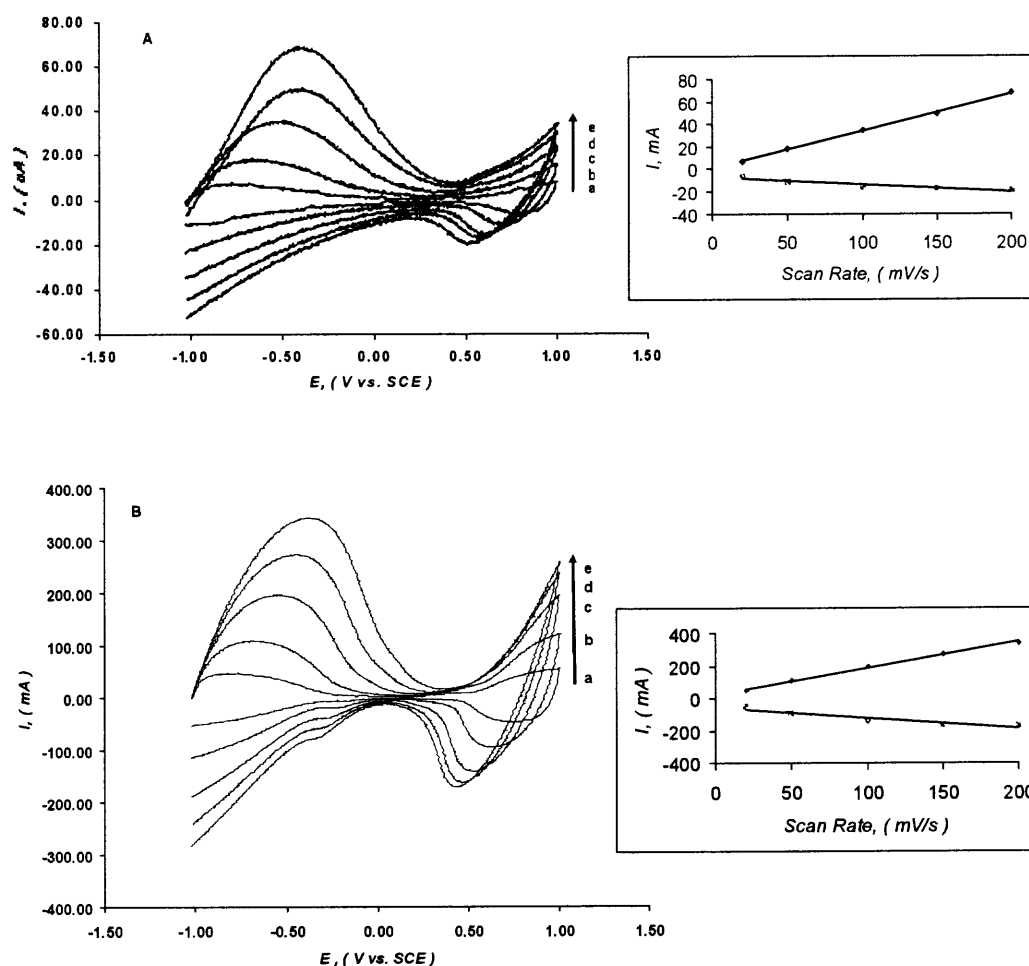

Figure 6.10 (A) CV curves of laccase deposition and the plots of redox peak currents versus scan rate on p-Si/MWNTs substrate (A), and p-Si/SWNTs substrate (B) at various scan rates (mV/s): a. 20, b. 50, c. 100, d. 150 and e. 200 mV/s. P-Si/CNT substrates are immersed in 20 ml buffer solution at pH 7.0, with 1mg/ml laccase.

The well-defined CV peaks (see Figure 6.10) indicated the occurrence of effective electrochemically-induced adsorption of laccase. The immobilization of laccase onto p-Si/MWNTs and p-Si/SWNTs involves electrochemical and chemical reactions of laccase coupling with CNTs by amide linkages similar to those observed for GOx and with CNTs.

The anodic and cathodic peak potentials of p-Si/MWNTs/laccase at a scan rate of 200 mV/s are -386 and 507 mV. A p-Si/SWNT/laccase electrode had redox peaks of -337 and 409 mV, for oxidation and reduction respectively. Their formal potentials at a scan rate of 200 mV/s were 51 mV and 34 mV for p-Si/MWNTs/laccase and p-Si/SWNTs/laccase, respectively. The anodic and cathodic peak currents were linearly proportional up to a scan rate of more than 200mV/s; it can be seen that the peak currents increase along with increase of scan rate, while ΔE_p values were reduced. The ΔE_p of p-Si/MWNTs/laccase and p-Si/SWNTs/laccase electrodes were 893 mV and 746 mV, at a scan rate of 200mV/s, both ΔE_p values were larger than 59mV, indicating that the systems are quasi-reversible with low electron transfer. This observation is similar to that observed for GOx immobilization. The lower ΔE_p of p-Si/SWNTs/laccase electrodes compared to p-Si/MWNTs/laccase electrodes was also found, which confirmed that SWNTs have more efficient electron transfer.
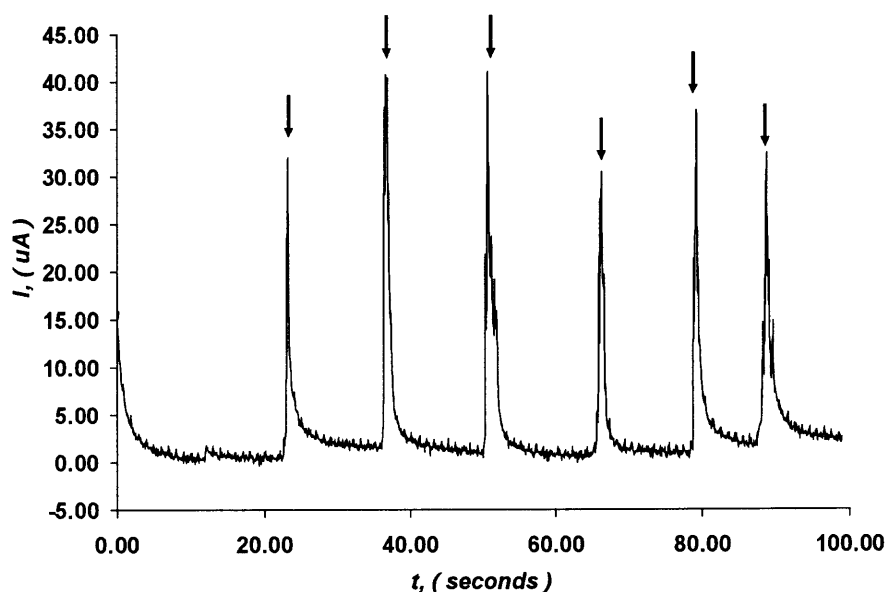
Figure 6.11 Amperometric responses of p-Si/MWNTs/laccase electrode at 300 mV in 20 ml pH 7.0 phosphate buffer, 0.1 M KCl upon additions of 2 ml of bubbled air.

Figure 6.11 shows the current surges obtained by additions of air to a p-Si/MWNT/laccase electrode at around 15 second intervals and a constant applied potential of 300 mV. The peaks were very sharp indicating that laccase immobilized on MWNTs was stable and corresponded to the reproducible biocatalytic reduction of O_2 to H_2O.

6.4   Set-up and Performance of Membrane-less Biofuel Cell

Two sets of electrodes: p-Si/MWNTs/GOx | p-Si/MWNTs/laccase and p-Si/SWNTs/GOx | p-Si/SWNTs/laccase were assembled to form membrane-less biofuel cells in order to evaluate their current-voltage and power output performance. The biofuel cell performance was obtained at a concentration of 4 mM glucose in pH 7.0 phosphate

buffer with constant stirring and air bubbling; the 1 cm by 1 cm anode and cathode

electrodes were positioned 5 mm apart by clamps (see Figure 6.12).
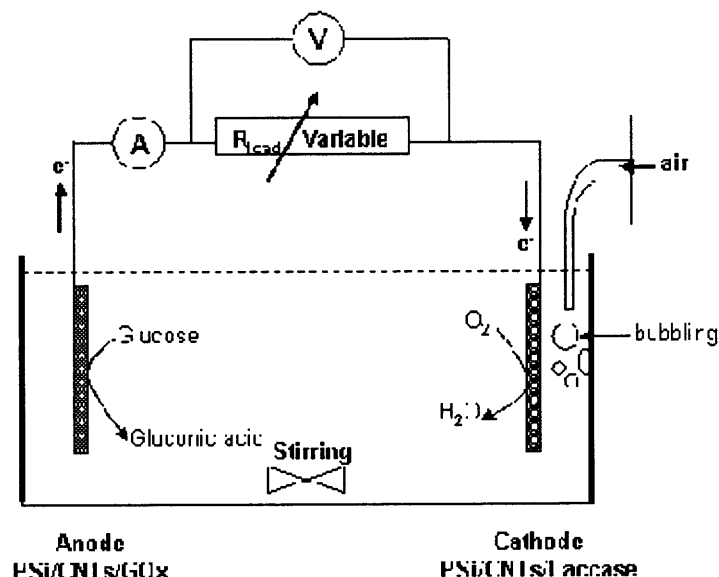
Figure 6.12 Schematic configuration of a biofuel cell employing glucose and O_2 as a fuel and oxidizer, respectively, and p-Si/CNTs/GOx and p-Si/CNTs/laccase functional electrodes as the biocatalytic anode and cathode, respectively. The distance between the two electrodes was 5 mm. The biofuel cell performance test was performed at 25 °C. The electrolyte contained 4 mM glucose and was constantly stirred under air flow during the tests.
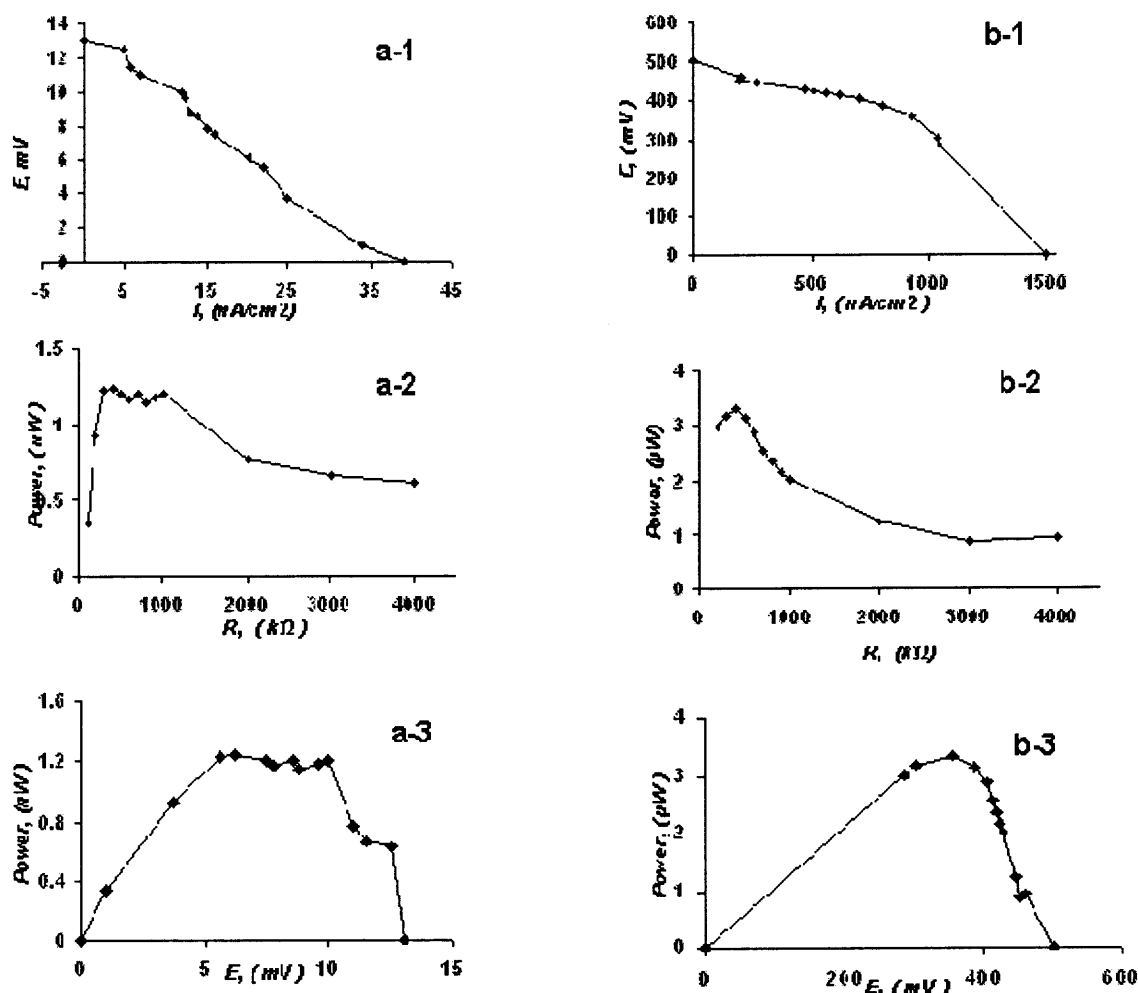
Figure 6.13 Current-voltage behavior of the biofuel cells, (a-1) and (b-1). Electrical power extracted from the biofuel cell at different external loads, (a-2) and (b-2). Electrical power vs. voltage plots, (a-3) and (b-3). The plots marked 'a' are from p-Si/MWNTs/GOx | p-Si/MWNTs/laccase biofuel cell, and the plots marked 'b' are from p-Si/SWNTs/GOx | p-Si/SWNTs/laccase biofuel cell.

Figure 6.13, (a-1) and (b-1) showed the current-voltage behavior of the biofuel cells (see

Figure caption) at different external loads. The ideal current-voltage relationship for an

electrochemical generator of electrical power is rectangular [11]. The p-Si/MWNTs/GOx

| p-Si/MWNTs/laccase biofuel cell showed a significant deviation from ideal behavior,

while p-Si/SWNTs/GOx | p-Si/SWNTs/laccase biofuel cell current-voltage relationship

trended rectangular. The extractable power from the biofuel cell (P=V_{cell} I_{cell}) is

controlled by the cell voltage (V_{cell}) and cell current (I_{cell}). The power (P) yield from the biofuel electrodes is shown in Figure 6.13 (a-2) and (b-2) for different external loads. The maximum power correspond to 1.24 μW for p-Si/MWNTs/GOx | p-Si/MWNTs/laccase biofuel cell at an external load of 400 kΩ with potential of 6.2 mV versus SCE, and 3.2 μW for p-Si/SWNTs/GOx | p-Si/SWNTs/laccase biofuel cell at an external load of 400 kΩ with 357 mV versus SCE. The fill factor, $f=P_{max} I_{sc}^{-1} v_{oc}^{-1}$, corresponds to ca. 26% and 44% for p-Si/MWNTs/GOx | p-Si/MWNTs/laccase and p-Si/SWNTs/GOx | p-Si/SWNTs/laccase biofuel cells respectively. The output of p-Si/SWNTs/GOx | p-Si/SWNTs/laccase biofuel cell compared fairly well with an output of 4 μW/cm^2 at 600 mV observed by Katz et al [11] for their glucose–O_2 biofuel operating in physiological solutions and based on a glucose oxidase anode and a cytochrome c/cytochrome c oxidase cathode.

Table 6.1 Characteristic Parameters of Biofuel Cells Based on p-Si/CNTs Electrodes with Immobilized GOx and Laccase

Biofuel cell	Open circuit voltage, mV	Short Circuit Current, nA	Maximum electrical power	Optimal loading resistance, kΩ	Optimal operating voltage, mV	Fill factor
p-Si/MWNTs/GOx, laccase	13	39	1.23nW	300	5.6	26%
p-Si/SWNTs/GOx, laccase	502	1500	3.32μW	400	357	44%

Comparing the characteristic parameters of the biofuel cells listed in Table 6.1, it was found that biofuel cell with p-Si/SWNTs/enzyme electrode had better performance than the one with MWNT-based electrodes. Table 6.2 lists some of the great strides that

have been made over the last few years in improving the current (and therefore power)

densities obtainable at electrodes using enzymatic-based biofuel cells.

Blank Page

CHAPTER 7

CONCLUSIONS

In summary, the author has demonstrated a new approach in this thesis for the fabrication of GOx and laccase-based biocatalysts on p-Si/CNTs substrates using a direct electrochemical technique. The promotion effects of CNTs (based on p-Si) on the direct electron transfer of GOx and laccase, which were immobilized onto the surface of CNTs, have been reported. Both SWNTs and MWNTs were used as direct electron transfer mediators. All cyclic voltammetric results showed a pair of well-defined redox peaks, which corresponded to the direct electron transfer to GOx and laccase enzymes. However the large separation potential between the redox peaks suggests that highly efficient direct electron transfer may require further changes in the design of the electrodes. One approach would be to use aligned SWNTs which may be the perfect material to achieve this goal. From the CV results, the p-Si/SWNTs electrode provided better electron transfer efficiency compared to the p-Si/MWNTs electrode. The chronoamperometry and chronopotentiometric experiments also demonstrated that the immobilized enzymes retained their bioelectrocatalytic activity: GOx had good responses to the additions of glucose where oxidation of glucose took place, and laccase had rapid responses to air involving the reduction of oxygen suggesting the potential use of these implantable electrodes as glucose and oxygen sensors. The method presented here can be easily extended to immobilize and obtain the direct electrochemistry of other enzymes.

Membrane-less biofuel cell performance was investigated for two sets of electrodes: p-Si/MWNTs/GOx | p-Si/MWNTs/laccase and p-Si/SWNTs/GOx | p-Si/SWNTs/laccase. Here SWNTs showed better electrical properties than MWNTs. The

power generated by the p-Si/SWNTs/GOx │ p-Si/SWNTs/laccase biofuel was higher than that of a p-Si/MWNTs/GOx │ p-Si/MWNTs/laccase biofuel cell by three orders of magnitude. One can therefore conclude that SWNT-based electrodes provide much better biofuel cell performance than electrodes based on MWNTs prepared by a similar method.

Blank Page

REFERENCES

1. Yahiro, A. T.; Lee, S. M. and Kimble, D. O., Bioelectrochemistry I "Enzyme Utilizing Biofuel Cell Studies" *Biochim. Biophys. Acta.* **1964,** 88, 375.

2. Drott, J.; Rosengren, L.; Lindstrom, K.; Laurell, T. "Pore Morphology Influence on Catalytic Turn-over for Enzyme Activated Porous Silicon Matrices" *Thin. Solid Films* **1998,** 330, 16.

3. Drott, J.; Lindstrom, K.; Rosengren, L.; Laurell, T. "Porous Silicon as the Carrier Matrix in Microstructured Enzyme Reactors Yielding High Enzyme Activities" *J. Micromech. Microeng.* **1997,** 7, 14.

4. Barton, S.C.; Gallaway, J.; Atanassov, P., "Enzymatic Biofuel Cells for Implantable and Microscale Devices" *Chem. Rev.* **2004,** 104, 4867.

5. Palmore, G. T. R.; Bertschy, H.; Bergens, S. H.; Whitesides, G. M. "Methanol/Dioxygen Biofuel Cells: Application of an Electro-Enzymatic Method to Regenerate Nicotinamide Adenine Dinucleotide" *J. Electroanal. Chem.* **1998,** 443, 155.

6. Pizzariello, A.; Pratt, K. F.E. J. "Theoretical Treatment of Diffusion and Kinetics in Amperometric Immobilized Enzyme Electrodes Part I: Redox mediator entrapped within the film" *Electroanal. Chem.* **1995,** 397, 61.

7. Kim, J.; Jia, H.; Wang, P. "Challenges in Biocatalysis for Enzyme-based Biofuel Cells" *Biotec Adv* **2006,** 24, 296.

8. Moore, C.M.; Akers, N.L.; Hill, A.D.; Johnson, Z.C.; Minteer, S.D., "Improving the Environment for Immobilized Dehydrogenase Enzymes by Modifying Nafion with Tetraalkylammonium Bromides" *Biomacromolecules* **2004,** 5, 1241.

9. Tarasevich, M.R.; Bogdanovskaya, V.A.; Zagudaeva, N.M.; Kapustin, A.V., "Composite Materials for Direct Bioelectrocatalysis of the Hydrogen and Oxygen Reactions in Biofuel Cells" *Russ J Electrochem* **2002,** 38,355.

10. Barton, S. C.; Kim, H.-H.; Binyamin, G.; Zhang, Y.; Heller, A. " Electroreduction of O_2 to Water on the Wired Laccase Cathode." *J. Phys. Chem.* **B2001,** 105, 11917.

11. Katz, E.; Willner, I.; Kotlyar, A. B. "A Non-compartmentalized Glucose | O2 Biofuel Cell by Bioengineered Electrode Surfaces" *J. Electroanal. Chem.* **1999,** 479, 64.

12. Katz, E.; Heleg-Shabtai, V.; Perez, M.A.; Teijelo, M. L.; Heahnel W. *Angew. Chem., Int. Ed.* **1998,** 37, 3253.

13. Jia, H.; Zhu, G.; Wang, P.; "Catalytic Behaviors Associated with Enzymes Attached to Nanoparticles: the Effect of Particle Mobility" *Biotechnol Bioeng* **2003**, 84, 406.

14. Dyal, A.; Loos, K.; Noto, M.; Chang, S. W.; Spagnoli, C.; Shafi, K. V. P. M; Ulman, A.; Cowman, M. and Gross, R. A.. "Activity of Candida Rugosa Lipase Immobilized on g-Fe₂O₃ Magnetic Nanoparticles" *J Am Chem Soc* **2003**, 125, 1684.

15. Jia, H.; In Book: Novel nanobiocatalysts for chemical processing and biofuel cells" THE UNIVERSITY OF AKRON, **2005.**

16. Withey, G.D.; Lazareck, A.D.; Tzolov, M.B.; Yin, A.; Aich, P.; Yeh, J.I.; Xu, J.M.; "Ultra-high Redox Enzyme Signal Transduction Using Highly Ordered Carbon Nanotube Array Electrodes" New focus. Biofuel cells. *Science* **2002**, 296.

17. Wang, P.; Dai, S.; Waezsada, S. D.; Tsao, A.; Davison, B. H. "Enzyme Stabilization by Covalent Binding in Nanoporous Sol-gel Glass for Nonaqueous Biocatalysis" *Biotechnol Bioeng* **2001**, 74, 249.

18. Chen, T.; Barton, S. C.; Binyamin, G.; Gao, Z.; Zhang, Y.; Kim, H-H. and Heller, A. "A Miniature Biofuel Cell" *J. Am. Chem. Soc.* **2001**, 123 (35), 8630.

19. Mano, N.; Mao, F.; Heller, A. "Characteristics of a Miniature Compartment-less Glucose-O2 Biofuel Cell and its Operation in a Living Plant" *J. Am. Chem. Soc.* **2003**, 125 (21), 6588.

20. Topcagic, S. and Minteer, S. D. "Development of a Membraneless Ethanol/oxygen Biofuel Cell" *Electrochimica Acta* **2006**, 51 2168.

21. Moore, C. M.; Minteer, S. D. and Martin R. S. "Microchip-based Ethanol/oxygen Biofuel Eell" *Lab Chip*, **2005**, 5, 218.

22. Dresselhaus, M.S.; Dresselhaus; G.; Avouris, P.; "Carbon Nanotube: Synthesis Structure, Properties and Applications Springer", *Topics in Applied Physics* Vol. **2001**, 80.

23. Harris, P. J. E. "*Carbon Nanotubes and Related Structures*", Cambridge University Press, **1999**.

24. Carbon nanotube page, Retrieved October 21 2006 from the World Wide Web: http://carbonnanotube.quickseek.com/.

25. A carbon nanotube page from Pennsylvania University, USA. Retrieved October 21 2006 from the World Wide Web: http://www.seas.upenn.edu/mse/research/nanotubes.html.

26. Iijima, S. "Helical microtubules of graphitic carbon" *Nature* **1991**, 354, 56.

27. Kroto, H.W.; Heath, J. R.; O'Brien, S. C.; Curl, R. F. and Smalley, R. E. "C_{60}: Buckminsterfullerene" *Nature* **1985**, 318, 162.

28. Kusaba, M.; Tsunawaki, Y. "Production of Single-wall Carbon Nanotubes by a XeCl Excimer Llaser Ablation" *Thin Solid Films* **2006**, 506, 255.

29. Maruyama, S.; Kojima, R.; Miyauchi, Y.; Chiashi, S.; Kohno. M. "Low-temperature Synthesis of High-purity Single-walled Carbon Nanotubes from Alcohol" *Chemical Physics Letters* **2002**,360, 229.

30. Dai, H.; "Carbon Nanotubes: Opportunities and Challenges" *Surface Science* **2002**, 500, 218.

31. Salvetat, J.-P.; Bonard, J.-M.; Thomson, N.H.; Kulik, A.J.; Forr´o, L.; Benoit, W.; Zuppiroli, L. "Mechanical Properties of Carbon Nanotubes" *Appl, Phys. A* **1999**, 69, 225.

32. Avouris, P. "Carbon Nanotube Electronics" *Chem. Phys.* **2002**, 281, 429.

33. Dekker, C. "Carbon Nanotubes as Molecular Quantum Wires" *Phys. Today* May, **1999.**

34. Ivnitski, D.; Branch, B.; Atanassov, P.; Apblett, C. "Glucose Oxidase Anode for Biofuel Cell Based on Direct Electron Transfer" *Electrochem. Comm.* **2006**, 8, 1204.

35. Cai, C.; Chen, J. "Direct Electron Transfer of Glucose Oxidase Promoted by Carbon Nanotubes" *Analy Biochem* **2004**, 332, 75.

36. Vo-Dinh, T "*Protein Nanotechnology – Protocols, Instrumentation, and Applications*" ISSN 1064-3745, Humana Press Inc. Totowa, NJ, **2005**, 10, 227.

37. Zhao, Y.; Zhang, W.; Chen, H. and Luo Q. "Derect Electron Transfer of Glucose Oxidase Molecules Adsorbed onto Carbon Nanotube Powder Microelectrode" *Anal Sci* **2002**, 18, 939.

38. Chen, L. and Lu, G. "Direct Electrochemistry and Electrocatalysis of Hybrid Film Assembled by Polyelectrolyte–surfactant Polymer, Carbon Nanotubes and Hemoglobin" *J Electroanal Chem* **2006**, 597, 51.

39. Liu,Y.; Qu, X.; Guo, H.; Chen, H.; Liu B. and Dong, S. "Facile Preparation of Amperometric Laccase Biosensor with Multifunction Based on the Matrix of Carbon Nanotubes–chitosan Composite" *Biosen & Bioelectro* **2006**, 21, 2195.

40. Chen, L. and Lu, G. "Direct Electrochemistry and Electrocatalysis of Hybrid Film Assembled by Polyelectrolyte–surfactant Polymer, Carbon Nanotubes and Hemoglobin" *J of Electroanal Chem* **2006**, 597, 51.

41. Lin, Y.; Lu, F.; Tu, Y. and Ren, Z. "Glucose Biosensors Based on Carbon Nanotube Nanoelectrode Ensembles" *Nano Lett* **2004**, 4, 191.

42. Sotiropoulou, S.; Chaniotakis, N. A. "Carbon Nanotube Array-based Biosensor" *Anal Bioanal Chem* **2003**, 375,103.

43. Zi, J.; Buscher, H.; Falter, C.; Ludwig, W. and Zhang, K. "Raman Shifts in Si Nanocrystals" *Appl. Phys. Lett.* **1996,** 69, 8.

44. Islam, M. N.; Pradhan, A. and Kumarb, S. "Effects of Crystallite Size Distribution on the Raman-Scattering Profiles of Silicon Nanostructures" *J. Appl. Phys.* **2005,** 98, 024309.

45. Iqbal, Z.; Veprek, S.; "Raman Scattering from Hydrogenated Microcrystalline and Amorphous Silicon" *J. Phys. C: Solid State Phys.* **1982**, 15, 377.

46. Jorio, A.; Pimenta, M. A.; Filho, A. G. S.; Saito, R.; Dresselhaus, G. and Dresselhaus, M. S. "Characterizing Carbon Nanotube Samples with Resonance Raman Scattering" *New J. Phys.* **2003,** 5 139.

47. A carbon nanotube page from Dr. Peter J F Harris at Department of Chemistry, University of Reading, UK. Retrieved October 10 2006 from the World Wide Web: http://www.personal.rdg.ac.uk/~scsharip/tubes.htm.

48. Canham, L. T. "Silicon Quantum Wire Array Fabrication by Electrochemical and Chemical Dissolution of Wafers" *Appl. Phys. Lett.* **1990**, 57, 1046.

49. Wrroyo-Hernandez, M.; Perez-Rigueiro, J.; Manso-Silvan, M. and Duart, J. M. M. "Biocativity Test for Amine-based Functionalized Meso and Macro-porous Silicon Substrates" *Mat. Sci. & Eng* **2006**, Article in Press.

50. Aravamudhan, S.; Rahman, A. R. A.; Bhansali, S.; "Porous Silicon Based Orientation Independent, Self- Priming Micro Direct Ethanol Fuel Cell" *Sensors and Actuators A* **2005,** 123, 497.

51. Wang, Y. Ph.D., *Thesis*, New Jersey Institute of Technology, Newark, NJ. **2005.**

52. Liu, J.; Rinzler, A. G., Dai, H. J.; Hafner, J. H.; Bradley, R. K.; Boul, P. J.; Lu, A.; Iverson, T.; Shelimov, K.; Huffman, C. B.; Rodriguez-Macias, F.; Shon, .; Lee, T. R.; Colbert, D. T.; Smalley, R. E. "Fullerene Pipes" *Science* **1998**, 280, 1253.

53. Murray, R. W., in A. J. Bard (Ed.), *Electroanalytic Chemistry*, Vol. 13, Dekker, New York, **1984**, p. 205.

54. Wang, R.; Xu, H.; Gao, L. and Liang J. "Growth of Single-walled Carbon Nanotubes on Porous Silicon" *Apl. Surf. Sci* **2005**, 13168, 5.

55. Kordas, K.; Pap, A. E., Vahakangas, J., Unsimaki, A. and Leppavuori, S. "Carbon Nanotube Synthesis on Oxidized Porous Silicon" *Apl. Surf. Sci* **2005**, 252, 1471.

56. Saito, R., Dresselhaus, G. and Dresselhaus, M.S. "Trigonal warping effect of carbon nanotubes" *Phys. Rev. B* **2000**, 61, 2981.

57. Greef, R.; Peat, R.; Peter, L. M.; Pletcher, D. and Robinson, J. *"Instrumental Methods in Electrochemicstry"* Ellis Horwood Limited, West Sussex, England, **1985**, 207.

58. Guiseppi-Elie, A.; Lei, C. and Baughman, R. H. "Direct Electron Transfer of Glucose Oxidase on Carbon Nanotubes" *Nanotech* **2002**, 13, 559.

59. Witt, S.; Wohlfahrt, G.; Schomburg, D.; Hecht, H. J. and Kalisz, H. M. "Conserved Arginine-516 of Penicillium Amagasakiense Glucose Oxidase is Essential for the Efficient Binding of β-D-glucose" *Biochem. J.* **2000**, 347, 553.

60. A webpage of *"Lipid Catabolism: Fatty Acids & Triacylglycerols"*, Retrieved October 24 2006 from the World Wide Web: http://www.rpi.edu/dept/bcbp/molbiochem/MBWeb/mb2/part1/fatcatab.htm.

61. Shleeva, S.; Perssona, P.; Shumakovichb, G.; Mazhugob, Y.; Yaropolovb, A.; Ruzgasa, T.; and Gorton, L. "Interaction of Fungal Laccases and Laccase-mediator Systems with Lignin" *Enzy & Microbial Tech* **2006**, 39, 841.

62. Frank Davisa, F.; Higson, S. P.J.; "Biofuel Cells — Recent Advances and Applications" *Biosen & Bioelectro* Accepted on 25 April **2006**, Article in Press.